uc3m | Universidad Carlos III de Madrid

Bachelor's Degree in Aerospace Engineering
2017-2018

Bachelor Thesis

Model Predictive Control Application to a Remotely Piloted Aircraft System (RPAS)'s Autopilot

---

PAU GAGO PADRENY

Tutor

Manuel Soler Arnedo

Leganés, 2018

Abstract

In recent years, the versatility of the Unmanned Aerial Vehicle (UAV) has translated into an increase in its range of applications. Border patrol, search and rescue, surveillance... are operations fixed wing typologies excel at. However, the introduction of fixed wing UAV is linked to the development of cost effective algorithms that implement advanced control schemes. In this project, a Model Predictive Control (MPC) control strategy is applied to the fixed wing mini-UAV Fulmar X. The proposed algorithm adopts a Receding Horizon approach that recalculates at each time instant a linear representation of aircraft dynamics. The performance of the controller is tested in a series of isolated manoeuvres that represent the expected aircraft operation envelope. This process leads to the definition of a set of control modules, on the basis of which it is possible to divide a complete flight mission into different segments. The results indicate that the controller behaves adequately throughout the nominal aircraft flight envelope, suppressing the instabilities associated with the presence of an unstable spiral mode and allowing for transitions of speed and altitude with an overshoot and a steady state error smaller than 1.3% and 0.30% respectively.

Keywords: Model Predictive Control, Optimal Control, Receding Horizon, UAV, Fixed Wing.

Acknowledgements

I would like to express my gratitude towards Manuel Soler Arnedo for the support and guidance provided throughout the completion of the project.

Likewise, I would like to extend my sincere thanks to Wake Engineering for providing the basis of a mathematical model of their UAV Fulmar X.

Finally, I would like to acknowledge the work of the UC3M Aerospace Engineering Group and the UC3M Library.

Contents

List of Figures

List of Tables

Chapter 1

Introduction

1.1 Motivation

The Unmanned Aerial Vehicle (UAV) is a growing business. Common as it is in the aerospace sector, these platforms originate from military programs. However, their proven versatility has found multiple applications in the civil sector. For instance, aerial mapping and topography, precision farming or operations in areas of difficult access, such as rescue exercises and insurance or industrial inspections. In quantitative terms, the amount of UAV models for military purposes raised from 413 in 2006, to 644 in 2016; in great contrast with the civil sector, raising from 124 to 1120 in the same time period [1].

Figure 1.1: Sanz / Skycatch, Christian. Industrial Inspection of Solar Panels. Digital image. Drones Are Becoming Energy's New Roustabouts. N.p., 21 Apr. 2014. Web. 16 June 2018.

However, the democratization of UAV has come together with some controversy, which is to be managed by proper regulation. In Spain, the first regulatory framework created by AESA dates back of 2014, which recognized a total of 335

official operators.[1] As of 23 April 2018, this number has increased to 3151 [2]. This is indicative of an incipient industry, consequence of a technology and a range of applications that evolve at great speed. In an effort to not fall back, the Spanish authorities updated the legal ground on 15 December 2017 [3]. Broadly speaking, the scope of this new regulation concerns UAV for civil applications with a take-off mass (TOM) below 150kg (unless regulated by UE policy), and UAV involved in police, traffic and customs police, search and rescue, firefighting and coastguard and similar operations, with no limitations of TOM. This decree describes the set of conditions under which the following applications are authorized: performance of night flights, flights over urban areas, flights in controlled airspace and usage restrictions applied to public institutions. Activities that were not permitted in 2016 [1].

Under this legal landscape we not only find official operators, but also design and manufacturing companies and Approved Training Organisations (ATO), adding up to more than 120 firms, the majority of which belong to the civil sector. Out of all these businesses, 70% have a workforce below 10 employees, and a 30% produce earnings above €500.000 [1].

Expanding the analysis to Europe, estimates for the future provided by [4] indicate that by 2035, a fleet of 395.000 professionally operated drones will account for a business volume of €10.000M, providing a total of 90.000 jobs.

Focusing on the platform itself, a wide variety of designs are available. Possibly the most popular typology is the multi-rotor, such as the quad-copter. This is due to their relative low cost and design simplicity, their hover capabilities (including vertical take-off and landing), and an eased operation that derives from their simplified controls. However, this design option does not perform optimally in high speed, long range operations, such as border surveillance. This market segment is a great opportunity for fixed wing UAV. The main issues that fixed wing aircraft face in their implementation as UAV are the increased complexity of the design, the costs of development and maintenance, and the absence of cost effective algorithms that implement advanced control schemes.

1.2 Objective

The objective of this project is to apply an unconventional control strategy to a RPAS. To this end, two task are executed:

- Identification and characterization of a fixed wing RPAS.
- Identification and application of an advanced control scheme.

1.3 State of the art

From the very beginning of aviation's history, the ability to control the aircraft has been at the core of the subject. The Wright brothers success is often-times

[1] More information here

attributed to their three-axis flight control system: broadly speaking, the elevator enabled the regulation of the aircraft's pitch, while the rudder, coupled with the anti-symmetrical warping (twisting) of the wings were in charge of heading and roll control.[2]

In their own words, as appears in the 14^{th} item in the Wright Brother's patent from 1906 [5]:

"A flying-machine comprising superposed connected aeroplanes, means for moving the opposite lateral portions of said aeroplanes to different angles to the normal planes thereof, a vertical rudder, means for moving said vertical rudder toward that side of the machine presenting the smaller angle of incidence and the least resistance to the atmosphere, and a horizontal rudder provided with means for presenting its upper or under surface to the resistance of the atmosphere, substantially as described."

This set of controls is essentially the same to the employed in conventional aircraft today. It allows the pilot to perform two different kind of actions. On the one hand, corrective activity to maintain the desired aircraft trajectory. On the other, commands to initiate a new manoeuvre. Great effort has been dedicated to the development of automatic flight control systems to take part in these loads.

The first notion of an autopilot is attributed to Lawrence Sperry on 1912, by traducing the readings of gyroscopic heading and attitude instruments to commands to the rudder and elevator. An improved version of it was part of the flight control system that led Wiley H. Post to complete the first solo flight around the world, on 1931.

The degree of sophistication of autopilots naturally increased overtime. A significant turning point was the introduction of computers in the flight control systems, when the size and weight of the hardware allowed it. Again, military and space programs led the development of the aerospace industry. As an example of that, the F-16, dating of 1978, sacrificed stability for an increased performance. This was allowed due to the corrective activity that was performed by the on-board computer "$MMC3000$", with a 12 MHz processor. The F-16 is still in service, and new versions have increased its computational power to about 400 MHz.[3] For a reference, this value is still an order of magnitude lower than the processing speed of an iPhone X.

Very much like stable and performing aircraft, not only powerful but also reliable and robust computers are required. And the concept of computer is not limited exclusively to the hardware, but also to its software.

Related to the software, possibly the most popular implemented control scheme is the PID controller. As in any type of controller, the objective is to determine the control law. In other words, upon receiving as input the current state of the aircraft, and the reference (desired) state, the controller produces a set of control actions to follow the reference state.

The control law of a PID controller has three components. One that is proportional to the difference between the current and the reference state (P). Another that is based on the time history of such difference (I) and the last that is

[2]More information here

[3]More information here

due to the current rate of change of it (D). This control algorithm is popular due to its apparent simplicity, a relatively good performance and a low computational cost.

Great effort has been put towards developing robust PID control. Several options are available in the market:

- "Vector", developed by "UAV Navigation".[4] Approximated selling price of $3000. Limited information available regarding the pricing.
- "Kestrel", by "Lockheed Martin"[5] Selling price of the autopilot: $5000. Ground control, datalink, antenna and other components are sold separately, which can increase the total cost to $20000.
- "Piccolo SL", by "UTC Aerospace Systems".[6] Approximated selling price above $12000. Limited information available regarding the pricing.

These products are integral solutions for the complete navigation system of the aircraft. They can be configured to include not only the PID software, but also the required sensors and interfaces. All the more reason for the reticence to shift towards more advanced control schemes.

However, there are a considerable amount of drawbacks. One of the most significant is its ability to deal with Multiple Input Multiple Output (MIMO) processes. For each of the output variables that wants to be controlled, there is an associated error signal (the difference between the reference and the current or measured state). The problem is then to, out of the all different error signals, obtain a single control law for each of the multiple inputs that satisfies the reference state of all the reference variables. This usually entails a complicated set of constraints amongst the different modules of a PID.

A satisfactory answer to this problem can be found in the realm of optimal control. Optimal control schemes are those that derive the corresponding control law according to the optimization of a predetermined objective function. For linear systems, with a quadratic objective functions, the LQ (linear quadratic) theory has been widely developed.

Linear Quadratic Regulator (LQR) and Model Predictive Control (MPC) are two different LQ problems. However, under certain conditions, the formulation of LQR and MPC can be made equivalent. The former was originated at the beginning of the LQ era, while the latter has been gaining popularity in the last decades.

Having explained the workings of a PID controller, the following comparison with LQ results. PID control focuses on past inputs to decide on future control actions, while LQ evaluates the effects that a current input will have in the future. This allows to construct a controller that anticipates and adapts to future events, bearing in mind the desired trajectory in future times, and the aircraft's current state.

The aforementioned PID controllers are developed for fixed wing UAV. This has allowed an increase of the number of fixed wing UAV in the civil sector in recent

[4]More information on Vector

[5]More information on Kestrel

[6]More information on Piccolo SL

years. An example of such is the 3.7 kg UAV WingtraOne,[7] developed for large coverage mapping; or the DV Wing,[8] a 940 grams UAV for precision farming.

These specimens are alternatives to a market segment with a significant presence of multi-rotor UAV. However, the competition vanishes in the surveillance operations, with requirements that the characteristics of fixed wing UAV satisfy better. For instance:

- DX-3. Developed by The Sky Guys, it has a maximum endurance of 25 hours, and a maximum mass of 46 kg, carrying 3 kg of payload.[9]
- Penguin B. Developed by UAV Factory, with a maximum endurance of 26.5 hours, and a maximum mass of 21.5 kg, carrying 4 kg of payload.[10]
- Fulmar X. Developed by Thales Group and Wake Engineering, it has a maximum endurance of 12 hours, with a maximum mass of 20 kg, carrying 8 kg of payload.[11]

In particular, the Fulmar X, which incorporates a PID controller, is currently in operation by the Malaysian Maritime Enforcement Agency, and has been recently acquired by the Spanish Marine Infantry.

Wake Engineering, for academic purposes, has provided the University Carlos III of Madrid information which allows to characterize the behaviour of the Fulmar X.

The control strategy Model Predictive Control will be applied to the Fulmar X. In a parallel Master's Thesis, Alejandro Torres Gamiz implements the LQR scheme to the same aircraft.

1.4 Methodology

The Model Predictive Control application to the UAV Fulmar X is detailed in the following bullet points:

1. Dynamic characterization of the UAV Fulmar.
2. Development of the theory behind Linear Model Predictive Control.
3. Application of the controller to a set of isolated manoeuvres. Sensitivity of the controller's performance with respect to its main of parameters.
4. Simulation of a complete flight mission.
5. Comparison of the response of MPC and LQR in a particular manoeuvre.

[7] More information on WingtraOne

[8] More information on DV Wing

[9] More information on DX-3

[10] More information on Penguin B

[11] More information on Fulmar X

Chapter 2

Aircraft Dynamics

2.1 Equations of Motion

The rigid body dynamics of a symmetric aircraft are represented by a well known set of differential equations. The process by which these equations can be derived is detailed in [6, Chapter 4]. Before presenting the mentioned set of equations, it is convenient to define the following reference frames:

- Earth Fixed reference frame. For the case at hand, it will be considered as an inertial reference frame, such that its origin and orientation remains constant over time.
- Body axes. These are axes that are attached to the aircraft, both in translation and rotation. The set of equations to be presented is directly applicable to any choice of body axes.
- Stability axes. These are a kind of body axes, particularly useful in the context of steady operation, as one of its directions is aligned with the reference velocity $\bar{v}$. These are the chosen body axes, with the following directions:
  - x axis: aligned with reference velocity $\bar{v}$.
  - y axis: out of the right wing.
  - z axis: down, through the belly – right handed reference frame.

Finally, the set of equations is as follows.

$$\begin{aligned} X - mg\sin\theta &= m(\dot{u} + qw - rv) \\ Y + mg\cos\theta\sin\phi &= m(\dot{v} + ru - pw) \\ Z + mg\cos\theta\cos\phi &= m(\dot{w} + pv - qu) \end{aligned} \tag{2.1.1}$$

$$\begin{aligned} L &= I_x\dot{p} - I_{zx}\dot{r} + qr(I_z - I_y) - I_{zx}pq \\ M &= I_y\dot{q} + rp(I_x - I_z) + I_{zx}(p^2 - r^2) \\ N &= I_z\dot{r} - I_{zx}\dot{p} + pq(I_y - I_x) + I_{zx}qr \end{aligned} \tag{2.1.2}$$

$$
\begin{aligned}
p &= \dot{\phi} - \dot{\psi}\sin\theta \\
q &= \dot{\theta}\cos\phi + \dot{\psi}\cos\theta\sin\phi \\
r &= \dot{\psi}\cos\theta\cos\phi - \dot{\theta}\sin\phi \\
\dot{\phi} &= p + (q\sin\phi + r\cos\phi)\tan\theta \\
\dot{\theta} &= q\cos\phi - r\sin\phi \\
\dot{\psi} &= (q\sin\phi + r\cos\phi)\sec\theta
\end{aligned}
\tag{2.1.3}
$$

$$
\begin{aligned}
\dot{x}_E &= u\cos\theta\cos\psi + v(\sin\phi\sin\theta\cos\psi - \cos\phi\sin\psi) \\
&\quad + w(\cos\phi\sin\theta\cos\psi + \sin\phi\sin\psi) \\
\dot{y}_E &= u\cos\theta\sin\psi + v(\sin\phi\sin\theta\sin\psi + \cos\phi\cos\psi) \\
&\quad + w(\cos\phi\sin\theta\sin\psi - \sin\phi\cos\psi) \\
\dot{z}_E &= -u\sin\theta + v\sin\phi\cos\theta + w\cos\phi\cos\theta
\end{aligned}
\tag{2.1.4}
$$

Where:

- The Equations (2.1.1) correspond to the balance of forces.
- The Equations (2.1.2) correspond to the balance of moments.
- The Equations (2.1.3) determine the evolution of the angular rates with time.
- The Equations (2.1.4) determine the evolution of the position of the aircraft with respect to the Earth Fixed frame.

Note that the set of Equations (2.1.2) limit the choice of body axes to those which contain two reference frame directions in the aircraft's plane of symmetry.

With respect to each of the terms that characterize the equations:

- The terms (X, Y, Z) include any force other than inertial or gravity contributions. In this project, it contains aerodynamic and control forces.
- The terms (L, M, N) refer to aerodynamic and control moments.
- The terms (u, v, w) correspond to the speed along the (x, y, z) stability axes. No wind velocity is considered.
- The terms (p, q, r) correspond to the angular rates about the (x, y, z) stability axes.
- The terms (ψ, θ, ϕ) are the Euler angles, corresponding respectively to the azimuth, elevation, and bank angles.
- The terms (x_E, y_E, z_E) correspond to the position of the aircraft respect to the Earth Fixed axes.

The above equations are a coupled non-linear ordinary differential system of equations. The scope of this analysis is restricted to a linear version of this set. Therefore, a linearisation is to be performed, in this case with respect to a reference condition of symmetric flight. This is done by adopting the typical small disturbances approach, by representing each variable as a sum of its reference value (indicated by a "0" in the sub-index) and a smaller order term representing the disturbance (indicated by a "Δ" in front):

- By choosing stability axes, the only non-zero component of velocity in the reference condition is u:
  - $u = u_0 + \Delta u$
  - $v = \Delta v$
  - $w = \Delta w$
- With respect to the angular variables:
  - $\phi = \Delta\phi$, due to a symmetric flight reference condition.
  - $\theta = \theta_0 + \Delta\theta$, where the reference elevation angle, due to the selection of stability axes, is interchangeable with the reference climb angle, if any.
  - $\psi = \Delta\psi$, where ψ_0 is set to zero for the sake of simplicity, since it does not invoke any dynamic effects.
  - $p = \Delta p$
  - $q = \Delta q$
  - $r = \Delta r$
- With respect to the forces and moments:
  - $X = X_0 + \Delta X$
  - $Y = \Delta Y$, symmetric flight.
  - $Z = Z_0 + \Delta Z$
  - $L = \Delta L$
  - $M = \Delta M$
  - $N = \Delta N$

In further sections, the variables with a reference condition equal to zero, will see its "Δ" dropped.

Before obtaining the linear set of equations, the incremental forces and moments need to be characterized. A well known linear model of such is provided in [6, Equations (4.9,17)], with approximations based on previous experience of the authors. The model is the following:

$$\begin{aligned}
\Delta X &= X_u \Delta u + X_w w + \Delta X_c \\
\Delta Y &= Y_v v + Y_p p + Y_r r + \Delta Y_c \\
\Delta Z &= Z_u \Delta u + Z_w w + Z_{\dot{w}} \dot{w} + Z_q q + \Delta Z_c \\
\Delta L &= L_v v + L_p p + L_r r + \Delta L_c \\
\Delta M &= M_u \Delta u + M_w w + M_{\dot{w}} \dot{w} + M_q q + \Delta M_c \\
\Delta N &= N_v v + N_p p + N_r r + \Delta N_c
\end{aligned} \tag{2.1.5}$$

The forces and moments are now expressed in terms of the so called stability derivatives and the deviation from the reference conditions. The process to fully characterize the stability derivatives is described in [6, Chapter 5 and Section 4.11]. For the concerning aircraft, the Fulmar, the required assumptions in this process are discussed further ahead in this Chapter.

Finally, by introducing (2.1.5) into (2.1.1)-(2.1.4), together with the small disturbance expansion of the variables, the uncoupled longitudinal and lateral aircraft dynamics are obtained, which can be expressed according to the typical structure of a State-Space representation:

$$\dot{x} = Ax + Bu \tag{2.1.6}$$

$$y = Cx + Du \tag{2.1.7}$$

with x representing the state vector, A the state matrix and B the control matrix. Equation (2.1.7) is the obervation equation, with y representing the selected output, C the output matrix, and D the feedforward matrix.

Longitudinal Dynamics

$$\begin{bmatrix} \Delta\dot{u} \\ \dot{w} \\ \dot{q} \\ \Delta\dot{\theta} \end{bmatrix} = \begin{bmatrix} \frac{X_u}{m} & \frac{X_w}{m} & 0 & -g\cos\theta_0 \\ \frac{Z_u}{m-Z_{\dot{w}}} & \frac{Z_w}{m-Z_{\dot{w}}} & \frac{Z_q+mu_0}{m-Z_{\dot{w}}} & \frac{-mg\sin\theta_0}{m-Z_{\dot{w}}} \\ \frac{1}{I_y}[M_u + \frac{M_{\dot{w}}Z_u}{m-Z_{\dot{w}}}] & \frac{1}{I_y}[M_w + \frac{M_{\dot{w}}Z_u}{m-Z_{\dot{w}}}] & \frac{1}{I_y}[M_q + \frac{M_{\dot{w}}(Z_q+mu_0)}{m-Z_{\dot{w}}}] & -\frac{M_{\dot{w}}mg\sin\theta_0}{I_y(m-Z_{\dot{w}})} \\ 0 & 0 & 1 & 0 \end{bmatrix} \begin{bmatrix} \Delta u \\ w \\ q \\ \Delta\theta \end{bmatrix} + \begin{bmatrix} \frac{\Delta X_c}{m} \\ \frac{\Delta Z_c}{m-Z_{\dot{w}}} \\ \frac{\Delta M_c}{I_y} + \frac{M_{\dot{w}}}{I_y}\frac{\Delta Z_c}{m-Z_{\dot{w}}} \\ 0 \end{bmatrix} \tag{2.1.8}$$

which allow to determine the two following kinematic variables:

$$\Delta\dot{x}_E = \Delta u\cos\theta_0 + w\sin\theta_0 - u_0\Delta\theta\sin\theta_0 \tag{2.1.9}$$

$$\Delta\dot{z}_E = -\Delta u\sin\theta_0 + w\cos\theta_0 - u_0\Delta\theta\cos\theta_0 \tag{2.1.10}$$

Lateral Dynamics

$$\begin{bmatrix} \dot{v} \\ \dot{p} \\ \dot{r} \\ \dot{\phi} \end{bmatrix} = \begin{bmatrix} \frac{Y_v}{m} & \frac{Y_p}{m} & \frac{Y_r}{m} - u_0 & g\cos\theta_0 \\ \frac{L_v}{I'_x} + I'_{zx}N_v & \frac{L_p}{I'_x} + I'_{zx}N_p & \frac{L_r}{I'_x} + I'_{zx}N_r & 0 \\ I'_{zx}L_v + \frac{N_v}{I'_z} & I'_{zx}L_p + \frac{N_p}{I'_z} & I'_{zx}L_r + \frac{N_r}{I'_z} & 0 \\ 0 & 1 & \tan\theta_0 & 0 \end{bmatrix} \begin{bmatrix} v \\ p \\ r \\ \phi \end{bmatrix} + \begin{bmatrix} \frac{\Delta Y_c}{m} \\ \frac{\Delta L_c}{I'_x} + I'_{zx}\Delta N_c \\ I'_{zx}\Delta L_c + \frac{\Delta N_c}{I'_z} \\ 0 \end{bmatrix} \tag{2.1.11}$$

which allow to determine the two following kinematic variables:

$$\dot{\psi}_E = r \sec \theta_0 \tag{2.1.12}$$
$$\Delta \dot{y}_E = u_0 \psi \cos \theta_0 + v \tag{2.1.13}$$

with

$$I'_x = (I_x I_z - I_{zx}^2)/I_z$$
$$I'_z = (I_x I_z - I_{zx}^2)/I_x$$
$$I'_{zx} = I_{zx}/(I_x I_z - I_{zx}^2)$$

2.2 UAV Fulmar X

The Fulmar X is a fixed wing mini-UAV (maximum mass below 25 kg) developed by Thales Group in collaboration with Wake Engineering. It is designed to perform in both the military and civil sector, covering a range of applications such as search and rescue operations, border patrol or surveillance and intelligence missions, offering up to 800 km of range at a cruise speed of 100 km/h. All the information can be consulted in its official website.[1]

Figure 2.1: Thales. Fulmar UAV on Launch Pad. Digital image. Thales: First Export of Spanish Mini-UAV Fulmar. N.p., 16 Mar. 2016. Web. 16 June 2018.

In terms of its set of controls, it does not follow a conventional configuration. Bearing in mind the mission requirements of the aircraft, not requiring high manoeuvrability, together with associated benefits of weight reduction, the design option followed was to opt for the use of elevons, combining in one single aerodynamic surface the function of elevator and ailerons. There are a total of two elevons, one on each wing. The left elevon can be seen in Figure 2.1, occupying

[1] Fulmar X Official English Webpage

over half of the semi-wing span, starting from the tip and going inboard. The sign criteria used defines the deflection of any of the elevons as positive when the motion is trailing edge down, and negative otherwise. This way, the symmetrical deflection of the elevons (both positive, or both negative) is similar to a conventional elevator, while its anti-symmetrical deflection (one positive, one negative) is similar to the conventional ailerons. The elevons constitute the only deflectable surface of the aircraft. The two vertical tails that emanate from each of the wing roots are non-movable surfaces.

The only other control incorporated is a propeller power unit. In Figure 2.1 the propeller unit can be identified by two black propeller blades placed at the tail of the fuselage, aligned with the direction of the wings at the time the image was taken.

2.3 Dynamical characterization

The objective of this section is to characterize each of the terms that appear on the linear system defined by Equations (2.1.8) and (2.1.11).

A total of three different sources were identified in Section 2.1:

- Inertial terms.
- Aerodynamic contribution. Characterized by stability derivatives.
- Control terms. Elevons and propulsive unit.

The expressions to account for each of these elements are described in [6, Chapters 4, 5]. Such expressions are ultimately related to the characteristics of the Fulmar, which are presented hereafter.

2.3.1 Inertia characterization

Table 2.1 summarises general data provided by Wake Engineering concerning the geometry and inertia of the aircraft with respect to its principal axes.

2.3.2 Aerodynamic characterization

The aerodynamic features of the Fulmar, particularly the non-dimensional stability derivatives, are obtained from an open source vortex lattice method. In particular, the AVL software.[2]

The software allows for the description of the aircraft geometric and mass characteristics as well as the aerodynamics of the lifting surfaces, including the elevons (control surfaces). The resulting executable program was provided by Wake Engineering to University Carlos III of Madrid, for academic purposes.

[2] http://web.mit.edu/drela/Public/web/avl/

Property	Value
MTOM (kg)	20
I_x (kg/m^2)	3.95
I_y (kg/m^2)	3.95
I_z (kg/m^2)	3.99
Wingspan (m)	3
Reference chord (m)	0.3751
Reference surface (m^2)	1.1254

Table 2.1: Geomety and Inertia of Fulmar X

To run the required simulations, the program receives as inputs the airspeed, the density (ISA altitude) and the deflection of the control surfaces. The output indicates the aerodynamic forces and moments, and the aerodynamic derivatives for such conditions. In order to satisfy the reference condition of steady symmetric flight, the resulting aerodynamic moments shall be null.

Therefore, the deflection of the control surface shall be iteratively changed to finally obtain the absence of moments. Due to the possibility to symmetrically deflect the elevons, the lateral moments can be made automatically equal to zero, for equal deflections of both surfaces. By running the simulation at a range of speeds and altitudes it is possible to characterize a flight envelope for the aircraft.

Mesh Generation

According to the information available in the official web page and to reunions held with Wake Engineering, the aircraft is able to perform up to an altitude of 3000 metres, and has a maximum speed of 150 km/h (approximately 42 m/s). The nominal cruise conditions are defined at an altitude of 400 metres and a speed of 100 km/h.

In order to obtain a satisfactory dynamical representation of the aircraft at a different set of conditions of speed and altitude, a program is developed to run the simulation for a range of altitudes from sea level to 2000 metres, and a range of airspeeds from 17.5 to 45 m/s. Altitudes greater than 2000 metres are not considered in order to obtain a finer grid in the altitudes where the aircraft is expected to operate the majority of the time.

A total of 360 different combinations of speed and altitude are calculated. The results of this simulations are stored to be loaded into the control unit. When it is required, in terms of the current speed and altitude, the controller estimates the

correspondent dynamics by linear interpolation in two variables. It must be noted that the variation of mass is not considered in the model. The simulations are all performed at the maximum take-off mass (20 kg).

By extending the lower bound of the speed to 17.5 m/s, manoeuvres of landing or climb, in which the forward speed may suffer significant changes, are more accurately described. Note that a climb manoeuvre at constant airspeed is also a condition of steady symmetric flight, so that the dynamics are still valid in that regime. The adopted model however is not a fair representation of the dynamics that occur during the transition between, for example, a steady level flight and a subsequent climb. The degree of reliability will depend on the magnitude of the deviation of the variables with respect to the reference value. An analysis of this feature is not performed in the report.

As it was mentioned previously, the process to obtain the aerodynamic derivatives in the required reference condition is an iterative one. This process is automated in the following way:

1. The AVL input file is rewritten with the desired speed and density. An initial value of 0 degrees is assigned to the deflection of the elevons. Run the first simulation.

2. Read the output file. Depending on the sign and magnitude of the pitching moment coefficient (lateral moments are null), increase or decrease the deflection of the elevons by an amount that ranges from 3 to 15 degrees. Write to file. Run the second simulation.

3. Read the output file. With the values of the pitching moment coefficient of the first and second simulations, and the elevon deflections that generated it, build a straight line. Estimate the value of the required elevon deflection to obtain zero pitching moment coefficient. Write to file. Run the third simulation.

4. Repeat number 3 until a total of 5 simulations are performed. The linear regression is performed only with the two most recent values of pitching moment coefficient and elevon deflection.

5. Save output file, which contains all the required information to characterize the aerodynamics of the aircraft at the specified combination of speed and density.

The option of performing the vortex lattice method simulation on-line was also considered, although discarded due to the heavy computational load it supposes.

2.3.3 Control's characterization

Elevons

The effect of the elevons is of an aerodynamic nature. In fact, the influence of the deflection of the elevon on the different vehicle variables can be constructed from the output of the AVL software.

However, since the elevons are responsible for both the function of an elevator and the ailerons, certain care must be taken. In the context of linear theory, it is assumed that the two possible modes of deflection of the elevons (symmetric and anti-symmetric) constitute two different independent controls, so that one mode of actuation does not constrain the other. Therefore, two different maximum amplitudes of deflection are selected, equal to $\pm 30°$.

In terms of rate of change, no data to model the reality is available, so that what is believed to be a conservative number is chosen, i.e. ± 5 degrees per second.

Propulsion unit

In this case, there is an absence of a proper characterization of the dependence of thrust with variables such as speed or altitude. As a consequence, a constant power propeller unit is assumed.

The only available information, provided by Wake Engineering is that it provides a maximum thrust corresponding to about 6 to 7 kg, which is approximately a third of the mass considered in the simulations. Therefore, a linear model of the throttle, between 0 and 1 is constructed, which similarly represents a linear variation between no thrust, and a third of the aircraft's weight.

In terms of rate of variation, again, bearing in mind estimates provided by Wake Engineering, it is assumed that the engine is able to increase its thrust delivery from null to maximum in a time period of 20 seconds.

2.4 Dynamic Stability

This section assesses the linear dynamic stability of the vehicle in terms of its longitudinal and lateral modes, extending to the whole envelope generated in Subsection 2.3.2, namely density in the range from 1.005 to 1.3 kg/m^3, and speed from 17.5 to 45 m/s.

Before proceeding to the results, it is necessary to acknowledge a series of limitations of the dynamical model.

1. There is limited information available to build a model of the controls.

2. The vortex lattice method does not allow for unsteady aerodynamics. On top of that, the unconventional aircraft's typology does not include a horizontal tail. Therefore, stability derivatives with respect to $\dot{\alpha}$ are not considered.

3. In the evaluation of the stability derivatives, [6, Chapter 5], partial derivatives with respect to the dynamic pressure, Mach number, or the thrust coefficient C_T are not evaluated due to the lack of data.

The results of the analysis indicate the presence of two longitudinal and three lateral modes throughout the whole envelope.

2.4.1 Longitudinal normal modes

Concerning the longitudinal modes, an eigenvalue analysis produces two complex conjugate pairs. The characteristics of each mode are displayed in the vector diagrams of Figure 2.2 (counter-clockwise angular velcity).

The figure on the left shows a mode characterized mainly by oscillations in the amplitude of the forward speed, u, and to a lesser degree by oscillations in the pitch angle, $\Delta\theta$, in spite of the fact of a light pitch rate q. Furthermore, the oscillations of u an $\Delta\theta$ are phased by 90°, such that an increase of the pitch angle in a quarter of oscillation from its reference value, θ_0, to its maximum positive $\Delta\theta$ is followed in the next quarter of oscillation by a deceleration to the absolute minimum $-\Delta u$. The opposite happens when the pitch angle decreases.

The right figure displays the second mode, dominated by oscillations in vertical speed w and the pitch rate, q with the former lagging 90° behind. In the context of linear theory, where a reference velocity u_0 is defined, the term vertical speed is used interchangeably with the term angle of attack, such that $\alpha \cong w/u_0$.

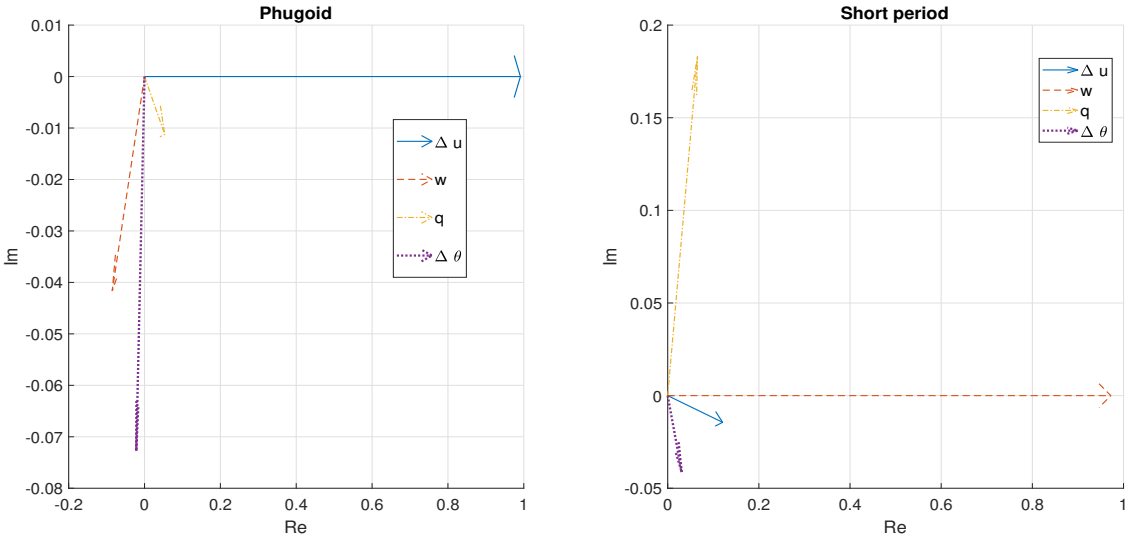

Figure 2.2: Vector diagram of the longitudinal normal modes.

These two oscillations are dynamically stable throughout the whole generated envelope. Particularly, the first mode described has a period and number of cycles to half amplitude that increase with speed, and decrease with altitude, Figure 2.3.

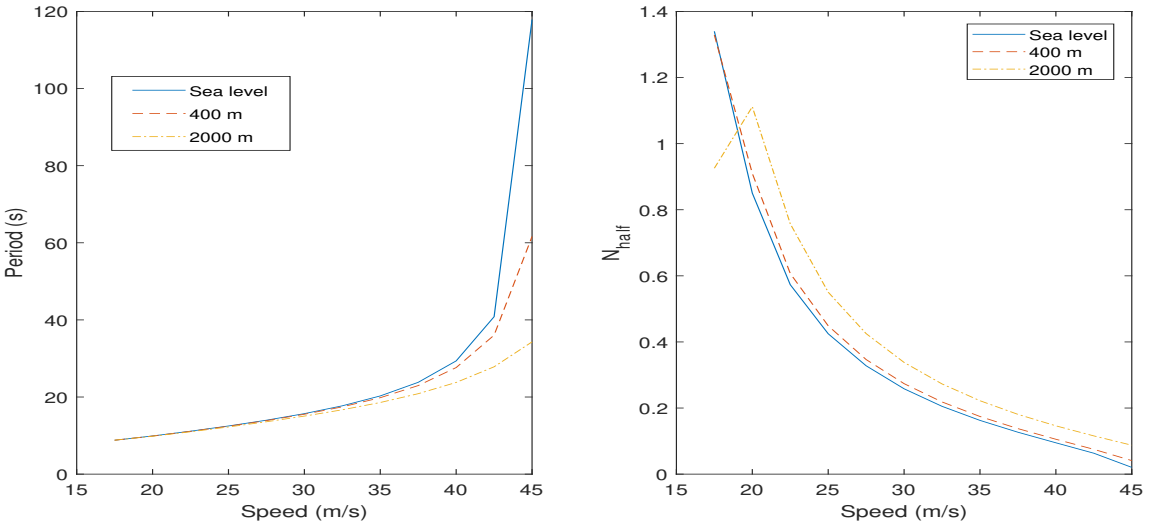

Figure 2.3: Variation of the phugoid mode with speed and altitude

The increase of the period with speed is particularly severe above speeds of 40 m/s, which is accompanied by a decrease in the number of cycles to half. These two facts are indicative of a tendency to shift towards marginal stability, or even to become unstable for high dynamic pressure. On the contrary, at low dynamic pressures, such as for a speed of 17.5 m/s at high altitudes such as 2000 metres, the vortex lattice method predicts a sudden decrease of the number of cycles to half.

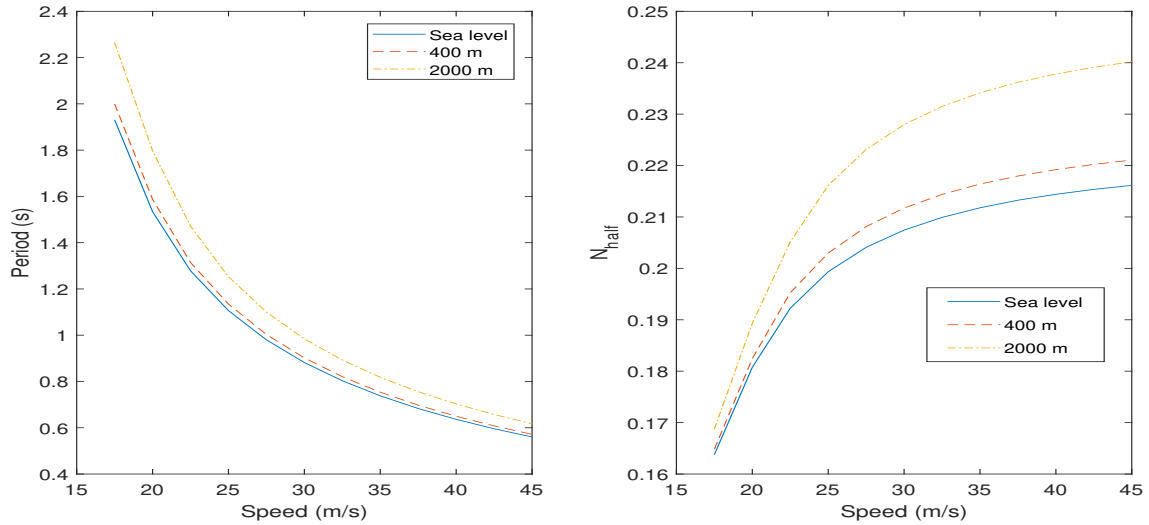

Figure 2.4: Variation of the short period mode with speed and altitude

The second mode, Figure 2.4, possesses a period and number of cycles to half that fall one order of magnitude lower, following also opposite evolution with speed and altitude than the first mode.

This information allows to identify these normal modes as the common aircraft phugoid and short period modes, respectively.

2.4.2 Lateral normal modes

Three different normal modes are identified across the whole flight envelope, with a single complex conjugate. Similarly to the longitudinal dynamics, these modes identify with the common roll convergence, dutch roll, and spiral modes. The dutch roll is mainly characterized by oscillations in the yaw rate r lagging 90° behind the lateral velocity v (or angle of sideslip, $\beta \cong v/u_0$), which can be seen in Figure 2.5. Regarding the dutch roll period, it is of the same order as the longitudinal short

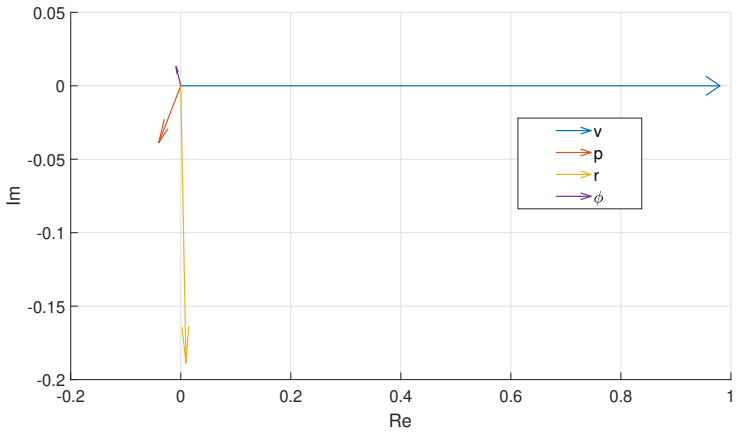

Figure 2.5: Vector diagram of the dutch roll mode

period. However, its behaviour presents a maximum at low speeds, approximately 2.1 seconds. See Figure 2.6.

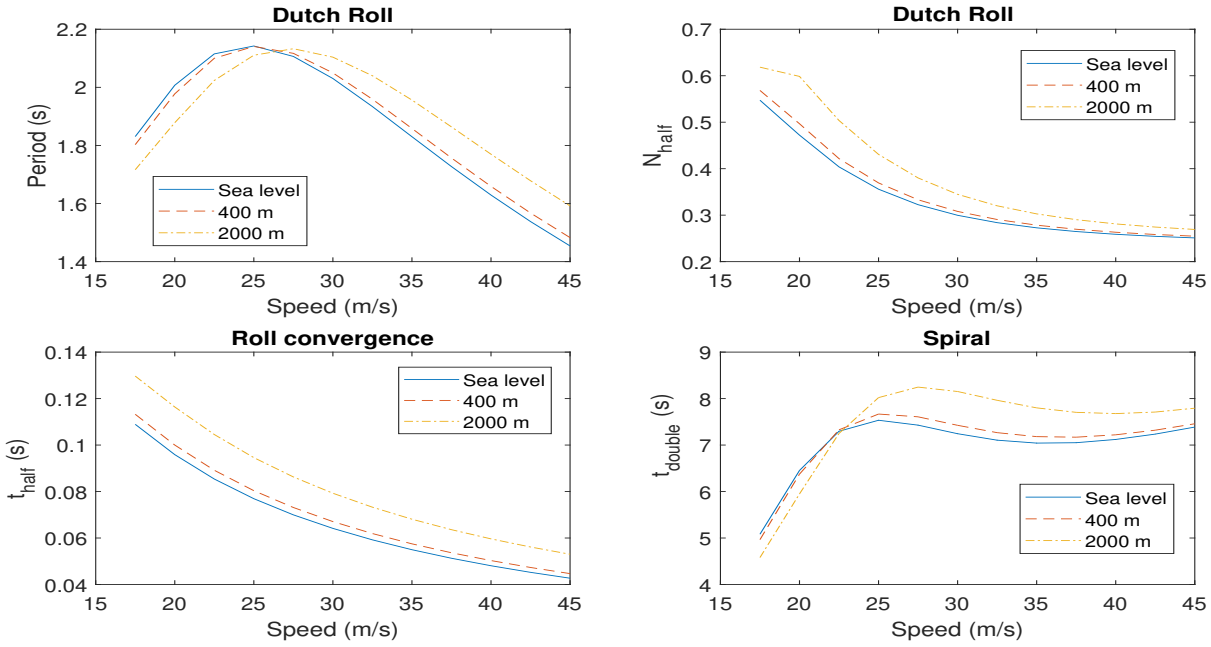

Figure 2.6: Variation of lateral normal modes with speed and height

The roll convergence is a highly damped mode, with a time to half amplitude of

the order of 0.1 seconds.

Finally, a dynamically unstable spiral mode is identified. This is a relatively slow mode however, with a time to double of approximately 7.5 seconds for a cruise condition of 28 m/s at 400 meters.

Chapter 3

Linear Model Predictive Control

3.1 Prediction Equation

Let us consider a MIMO system defined by Equations (2.1.6) and (2.1.7):

$$\dot{x} = Ax + Bu$$
$$y = Cx + Du$$

These equations are a linear, time invariant representation of the aircraft dynamics. Furthermore, they are expressed in continuous time.

However, the problem formulation will be performed in discrete time. This is convenient because it represents the actual operating conditions of the autopilot, since the value of the aircraft state variables are the result of the discrete sampling performed by the different sensors.

There are several discretization schemes. The one applied is known as zero-order hold (ZOH). This scheme assumes a step-function description of the variables in each sampling time period. Since only the value of the state and control variables at each sampling instant is required, and not in between sampling periods, a higher order method that produces a smooth variation between sampled values is not considered. In the Matlab environment, there is a functionality that performs the discretization, and as this feature does not belong to the scope of the project, it is not further investigated.

The equations of motion, in discrete time, have the following appearance:

$$x_{k+1} = Ax_k + Bu_k \tag{3.1.1}$$
$$y_k = Cx_k + Du_k \tag{3.1.2}$$

where the feed-forward matrix, D, is equal to zero in all type of operations considered for the controller.

Equation (3.1.1) now produces the state vector at time instant $k+1$, as a function of the current state vector, x_k and the control to be performed at this time instant,

u_k. This last term, u_k, is the unknown which is the responsibility of the controller to determine.

This same process can be reproduced for the next time instant:

$$x_{k+2|k} = Ax_{k+1|k} + Bu_{k+1}$$

Where the vertical bar denotes at which time instant, the indicated variable is predicted. Therefore, $x_{k+2|k}$ is the value of the state vector at time instant $k+2$, predicted at time instant k. Notice that the set of equations that represent the dynamics of the aircraft is a model of the true dynamics, and thus, the qualification of "predicted".

In this equation, the prediction for $x_{k+1|k}$ can be inserted, producing:

$$x_{k+2|k} = A^2x_k + ABu_k + Bu_{k+1}$$

Following this procedure, the prediction for the state vector at any given time instant $k+i$ is easily obtained:

$$\begin{aligned}
x_{k+1|k} &= Ax_k + Bu_k \\
x_{k+2|k} &= A^2x_k + ABu_k + Bu_{k+1} \\
x_{k+3|k} &= A^3x_k + A^2Bu_k + ABu_{k+1} + Bu_{k+2} \\
&\vdots \\
x_{k+N_p|k} &= A^{N_p}x_k + A^{N_p-1}Bu_k + A^{N_p-2}Bu_{k+1} + \\
&\quad + ... + ABu_{k+N_p-2} + Bu_{k+N_p-1}
\end{aligned}$$

Where the term N_p denotes the prediction horizon. It indicates the number of time instants ahead of k, for which the state vector is predicted.

These equations are now a function of a single state, which is the present state, x_k, and the sequence of controls up to time instant $k+N_p-1$, which can be considered as a vector of unknowns.

In principle, associated to each state vector, x_{k+i}, there is a corresponding control action u_{k+i-1} that is involved in its prediction. This means that the number of predictions for the state vector, from $k+1$ tp $k+N_p$ is equal to the dimension of control vector, with terms u_k to u_{k+N_p-1}, and both equal to N_p. However, as will be concluded in further sections, the number of control actions considered as unknowns has a significant impact on the computational load. Therefore, it is common to introduce the parameter known as control horizon, N_c, which indicates the number of time instants ahead of k, for which the control vector is to be determined. Control actions ahead of N_c, up to $N_p - 1$ are set to zero. Bearing this in mind, the new set of prediction equations can be written as follows:

$$\begin{aligned}
x_{k+1|k} &= Ax_k + Bu_k \\
x_{k+2|k} &= A^2x_k + ABu_k + Bu_{k+1} \\
x_{k+3|k} &= A^3x_k + A^2Bu_k + ABu_{k+1} + Bu_{k+2} \\
&\vdots \\
x_{k+N_p|k} &= A^{N_p}x_k + A^{N_p-1}Bu_k + A^{N_p-2}Bu_{k+1} + \\
&\quad + ... + A^{N_p-N_c+1}Bu_{k+N_c-2} + A^{N_p-N_c}Bu_{k+N_c-1}
\end{aligned}$$

Introducing each of the predicted states, from time instant $k+1$ to $k+N_p$, into Equation (3.1.2), the predicted output is obtained. This set of equations can be expressed in the following matrix form:

$$Y = Fx_k + \Phi U \tag{3.1.3}$$

where

$$Y = \begin{bmatrix} y_{k+1|k} \\ y_{k+2|k} \\ \vdots \\ y_{k+N_p|k} \end{bmatrix}, \; U = \begin{bmatrix} u_k \\ u_{k+1} \\ \vdots \\ u_{k+N_c-1} \end{bmatrix}$$

and

$$F = \begin{bmatrix} CA \\ CA^2 \\ \vdots \\ CA^{N_p} \end{bmatrix}, \; \Phi = \begin{bmatrix} CB & 0 & 0 & \dots & 0 \\ CAB & CB & 0 & \dots & 0 \\ CA^2B & CAB & CB & \dots & 0 \\ \vdots & & & & \\ CA^{N_p-1}B & CA^{N_p-2}B & CA^{N_p-3}B & \dots & CA^{N_p-N_c}B \end{bmatrix}$$

In the general case, for a MIMO system, the dimension of each of the terms depends on the selected prediction horizon, N_p, and control horizon, N_c. Assuming a n-state x, m-input u system, with a selected output y of dimension q, with $q \leq n$:

- $A \in \mathbb{R}^{n \times n}$
- $B \in \mathbb{R}^{n \times m}$
- $C \in \mathbb{R}^{q \times n}$

so that

- $Y \in \mathbb{R}^{q \cdot N_p}$
- $U \in \mathbb{R}^{m \cdot N_c}$
- $F \in \mathbb{R}^{q \cdot N_p \times n}$, where each of the entries is a matrix itself, of dimensions $q \times n$
- $\Phi \in \mathbb{R}^{q \cdot N_p \times m \cdot N_c}$, where each of the entries is a matrix of dimensions $q \times m$

This procedure has been developed according to the approach presented for SISO (Single Input Single Output) systems in [7, Chapter 1].

3.2 Optimization problem set up

Equation (3.1.3) constitutes the prediction equation. Knowing the current state, the output in future time instants is exclusively a function of the future sequence of controls. To determine it, an optimization problem is set up.

3.2.1 Performance metric

The first step is to build a cost function, which is a performance metric that weights the predicted output against a series of parameters. The expression below is a modified version of the one appearing on [7, Equation (1.13)], in order to include weights in the state, not only in the controls:

$$J = (Y - R_s)^T W (Y - R_s) + U^T \overline{R} U, \in \mathbb{R} \tag{3.2.1}$$

where the first term collects the deviation of the predicted output with respect to a reference trajectory, R_s, and the second reflects the severity of the controls to reduce it. The reference signal, R_s, is a vector with $N_p \cdot q$ entries, i.e. the value of each of the q output variables for every of the N_p time instants inside the prediction horizon. The relative impact on the cost function J of each term is modulated by two different weighting terms, W and $\overline{R}$.

With respect to W, weighting the first term, two popular structures are proposed in [8, Chapter 2]:

- Constant weighting. A single scalar can be assigned, or else a diagonal matrix $W \in \mathbb{R}^{N_p \cdot q \times N_p \cdot q}$ can be build, in which a total of q different constants are defined, one for every output variable. Those q values are repeated N_p times, one for every predicted time instant.

- Exponential weighting, $W \in \mathbb{R}^{N_p \cdot q \times N_p \cdot q}$ is a diagonal matrix. In this case, the difference between the reference signal and the predicted output can be given different importance at different time instants. Therefore, for a given output variable $y(j)$, with $j \leq q$, its weighting factor at time instant $k+i$, $i \leq N_p$, is $W(q \cdot (i-1)+j, q \cdot (i-1)+j) = \alpha^{N_p - i}$. For $\alpha > 1$, the differences at the initial times penalize more than the final ones. The opposite happens for $\alpha < 1$.

For the case of $\overline{R}$, only constant weighting is considered in this project. For the sake of completeness, $\overline{R} \in \mathbb{R}^{N_c \cdot m \times N_c \cdot m}$

Concerning the reference signal, $R_s \in \mathbb{R}^{N_p \cdot q}$, it contains the desired future value of each of the q output variables at each of the N_p time instants ahead of the current one.

Now that every term is characterized, Equation (3.2.1) can be treated to adopt the typical expression of a quadratic optimization problem.

3.2.2 Quadratic Programming

A typical representation of a quadratic programming problem is the following:

$$\begin{aligned} \min_{x} \quad & \frac{1}{2} x^T H x + x^T g \\ s.t. \quad & A_{lb} \leq Ax \leq A_{ub} \\ & lb \leq x \leq ub \end{aligned} \tag{3.2.2}$$

where the decision variable, x, corresponds to the vector of controls U; lb and ub impose amplitude constraints; and A_{lb} and A_{ub} will be used to impose rate

constraints. The matrix A is not the state matrix from Equation (3.1.1). This notation is used due to its generality.

The rest of the section is dedicated to finding expressions for matrix H and vector g to define the problem statement, as well as to characterize the constraints.

Cost function

Introducing Equation (3.1.3) into Equation (3.2.1):

$$J = (Fx_k + \Phi U - R_s)^T W (Fx_k + \Phi U - R_s) + U^T \overline{R} U$$

and collecting the terms inside of the brackets that do not depend on the decision variable U:

$$\begin{aligned} J = {} & (Fx_k - R_s)^T W (Fx_k - R_s) + (Fx_k - R_s)^T W \Phi U + (\Phi U)^T W (Fx_k - R_s) \\ & + (\Phi U)^T W \Phi U + U^T \overline{R} U \end{aligned}$$

The first term does not depend con the optimization variable U, and thus it does not go into the resolution of the quadratic programming problem. Recalling the properties of matrices, $(ABC)^T = C^T B^T A^T$, the expression is reorganized:

$$\begin{aligned} J = {} & f(x_k, R_s) + (Fx_k - R_s)^T (U^T \Phi^T W^T)^T + U^T \Phi^T W (Fx_k - R_s) \\ & + U^T \Phi^T W \Phi U + U^T \overline{R} U \\ & = f(x_k, R_s) + (U^T \Phi^T W^T (Fx_k - R_s))^T + U^T \Phi^T W (Fx_k - R_s) \\ & + U^T (\Phi^T W \Phi + \overline{R}) U \end{aligned}$$

Finally, by realizing that W is a diagonal matrix, and that J is a scalar, its dimensions and value are not changed by the transpose operation:

$$\begin{aligned} J = {} & f(x_k, R_s) + U^T \Phi^T W (Fx_k - R_s) + U^T \Phi^T W (Fx_k - R_s) \\ & + U^T (\Phi^T W \Phi + \overline{R}) U \\ & = f(x_k, R_s) + 2U^T \Phi^T W (Fx_k - R_s) + U^T (\Phi^T W \Phi + \overline{R}) U \end{aligned}$$

obtaining by analogy to Equation (3.2.2) the expressions for matrix H and g:

$$H = 2(\Phi^T W \Phi + \overline{R}), \quad \in \mathbb{R}^{N_c \cdot m \times N_c \cdot m} \tag{3.2.3}$$

$$g = 2\Phi^T W (Fx_k - R_s), \quad \in \mathbb{R}^{N_c \cdot m} \tag{3.2.4}$$

Constraints

Bearing in mind the capabilities of the aircraft defined on Subsection 2.3.3, two kind of constraints on the control U are implemented.

The vectors lb and ub impose a lower and upper bound to the amplitude range of each control. The dimension of these vectors is $N_c \cdot m$, equal to the dimension of the control vector U. By defining the terms u^{min} and $u^{max} \in \mathbb{R}^m$ containing

the minimum and maximum values of each entry of the control vector for any time instant, the amplitude inequality is defined as follows:

$$\begin{bmatrix} u^{min} \\ u^{min} \\ \vdots \\ u^{min} \end{bmatrix} \leq \begin{bmatrix} u_k \\ u_{k+1} \\ \vdots \\ u_{k+N_c-1} \end{bmatrix} \leq \begin{bmatrix} u^{max}, \\ u^{max} \\ \vdots \\ u^{max} \end{bmatrix} \tag{3.2.5}$$

If the bounds of the above inequality are applied to each of the N_c control terms that make up the control vector U, the amplitude constraint lb and ub are defined.

Concerning the rate constraints in discrete time, the approach is to limit the difference between consequent time steps:

$$\begin{aligned} \Delta u^{min} \leq\ & u_k - u_{k-1} \leq \Delta u^{max} \\ \Delta u^{min} \leq\ & u_{k+1} - u_k \leq \Delta u^{max} \\ & \vdots \\ \Delta u^{min} \leq\ & u_{k+N_c-1} - u_{k+N_c-2} \leq \Delta u^{max} \end{aligned}$$

where Δu^{min} and $\Delta u^{max} \in \mathbb{R}^m$ contain the minimum and maximum rates of each control.

This set of inequalities can not yet be expressed as it is required, meaning a single expression of the form $A_{lb} \leq Ax \leq A_{ub}$, due to the presence of u_{k-1} in the first line, which is a known term corresponding to the control law applied in the previous time step $k-1$. By adding the term u_{k-1} to the first line, only terms related to U are obtained at the centre of each inequality:

$$\begin{aligned} \Delta u^{min} + u_{k-1} \leq\ & u_k \leq \Delta u^{max} + u_{k-1} \\ \Delta u^{min} \leq\ & u_{k+1} - u_k \leq \Delta u^{max} \\ & \vdots \\ \Delta u^{min} \leq\ & u_{k+N_c-1} - u_{k+N_c-2} \leq \Delta u^{max} \end{aligned}$$

So that it can be expressed in a compact form:

$$\begin{bmatrix} \Delta u^{min} \\ \Delta u^{min} \\ \vdots \\ \Delta u^{min} \end{bmatrix} + \begin{bmatrix} I_{m\times m} \\ 0 \\ \vdots \\ 0 \end{bmatrix} u_{k-1} \leq \begin{bmatrix} I_{m\times m} & & & \\ -I_{m\times m} & I_{m\times m} & & \\ & & \ddots & \\ & & -I_{m\times m} & I_{m\times m} \end{bmatrix} U \leq \begin{bmatrix} \Delta u^{max} \\ \Delta u^{max} \\ \vdots \\ \Delta u^{max} \end{bmatrix} + \begin{bmatrix} I_{m\times m} \\ 0 \\ \vdots \\ 0 \end{bmatrix} u_{k-1} \tag{3.2.6}$$

where the vectors A_{lb} and A_{ub}, and the matrix A can be obtained by analogy with Equation (3.2.2).

3.2.3 Problem Statement

The resulting optimization problem is summarized hereafter:

$$\min_{U} \qquad U^T(\Phi^T W \Phi + \overline{R})U + 2U^T \Phi^T W(Fx_k - R_s) \tag{3.2.7}$$

subjected to (3.2.5) and (3.2.6).

All elements required to implement a Model Predictive Control control strategy have been defined. These are put together in an iterative routine as shown in the following section.

3.3 Algorithm

The algorithm to be developed has the objective of providing a solution to the following statement: given the current state and the desired future trajectory, obtain the control law to follow.

Knowing the current state, the dynamics of the aircraft can be interpolated in speed and altitude obtaining the matrices A and B of Equation (2.1.6). Therefore, matrices F and Φ of the prediction Equation (3.1.3) are also known. These two matrices, together with the reference signal R_s fully determine the statement of the quadratic programming problem. On the other hand, the past control action is also known, which allows to update the rate constraints.

These terms are passed on to a quadratic programming solver. Particularly, the open source solver "qpOASES"[1] is chosen, due to its Matlab interface with the ability of C-Code generation for future platform integration. The output of this function is the optimal control law U.

The next step of the process is to select the control actions to be applied to the system. This is because U contains a total of N_c consecutive commands. Adopting the concept of receding horizon, only the first control action is selected, this is, u_k.

Finally, Equation (3.1.1) is used to determine the next state.

This completes one iteration of the algorithm. It is illustrated below:

[1] https://projects.coin-or.org/qpOASES

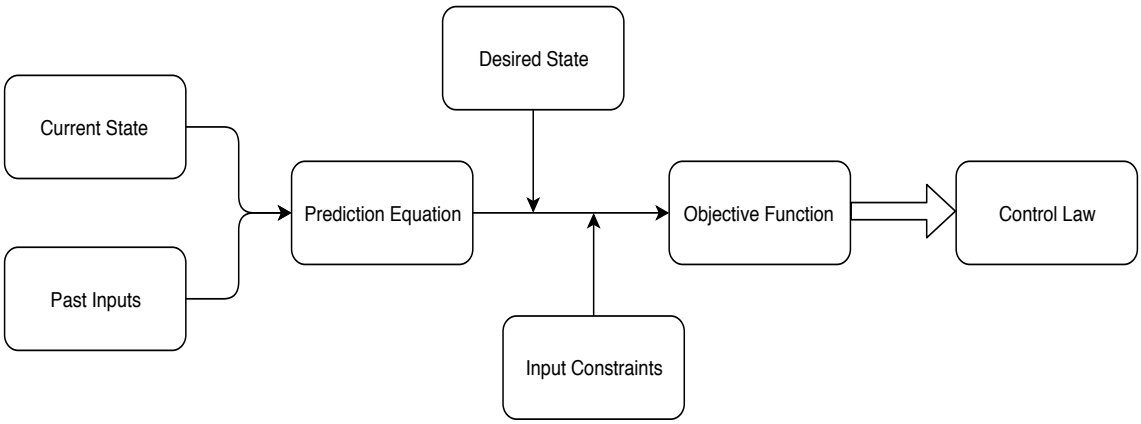

Figure 3.1: MPC iterative algorithm

Chapter 4

MPC in isolated manoeuvres

The objective of this chapter is to test the performance of Model Predictive Control in a set of single manoeuvres. On the one hand, the aircraft will be subjected to disturbances that excite its normal modes, particularly the phugoid and the spiral mode. On the other hand, the ability of the controller to transition between equilibrium states in terms of changes in the cruise speed, altitude and heading will be assessed.

4.1 Stability augmentation

All simulations in this section are performed at a reference altitude of 400 metres and speed of 28 m/s, corresponding to the nominal operation of the aircraft. The dynamics of the aircraft, matrices A and B of Equation (3.1.1), are held constant, not resorting to the mesh generated.

4.1.1 Phugoid suppression

Considering the longitudinal dynamics of the Fulmar as described by Equation (2.1.8) and the kinematic expression to determine the variation in altitude (2.1.10), an augmented system is built, by introducing the variables Δz_E into the state vector x_{long}, such that:

$$x_{long} = \begin{bmatrix} \Delta u \\ w \\ q \\ \Delta\theta \\ \Delta z_E \end{bmatrix}$$

where z_E is interchangeable with h.

Note that this is a purely kinematic variable, and thus does not affect the dynamic stability of the aircraft. From a mathematical standpoint, the rank of the augmented state matrix A_{long} is equal to 4.

The uncontrolled response to a disturbance that excites the phugoid mode (at this particular speed and altitude) is shown in Figure 4.1. The behaviour of the

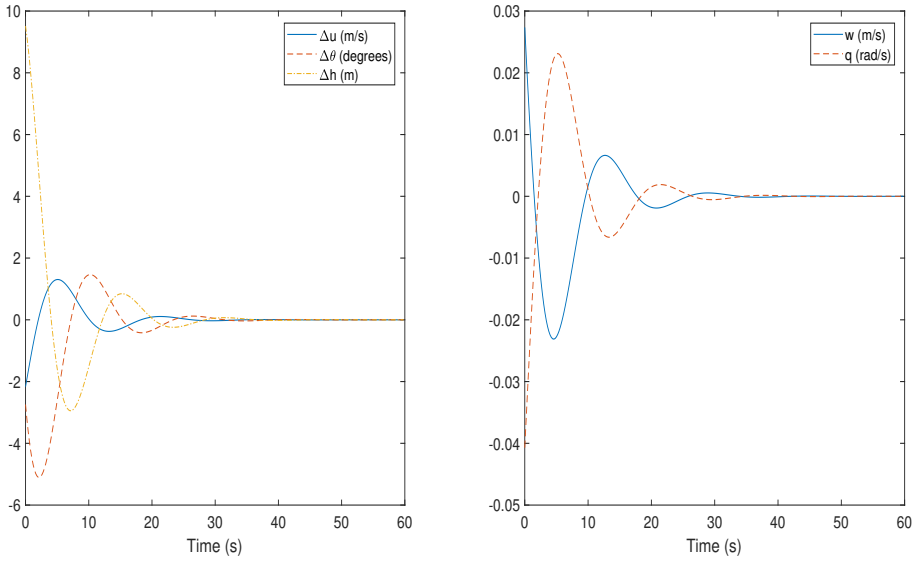

Figure 4.1: Phugoid mode. No controls.

aircraft, after a disturbance of $\Delta u \approx -2$ m/s, and of 10 metres in altitude, follows an oscillatory recovery to equilibrium. Particularly, the speed reaches an overshoot of 60% the magnitude of the initial disturbance, and an overall range of variation equal to 12% of the nominal cruise speed. These numbers might constitute a hazard during certain phases such as landing, operating close to stall. Regarding the oscillations in altitude, these remain within a 2% of the initial disturbance after 25.1 seconds.

A controller is designed with the following parameters:

- Sampling rate $\Delta t = 0.2$ seconds.
- Prediction horizon $N_p = 50$.
- Control horizon $N_c = 12$.

According to the first two points, the prediction equation extends $N_p \cdot \Delta t = 10$ seconds ahead of the time instant at which it is calculated. Concerning the output, every variable of the state vector is observed, meaning that matrix C of Equation (3.1.2) is equal to the identity matrix $I_{5\times5}$. As was mentioned above, matrix D has its entries equal to zero.

Regarding the reference signal R_s, it is equal to zero for each of the output

variables. Therefore, at a given time instant $k+i \leq N_p$:

$$R_s|_{k+i} = \begin{bmatrix} 0 \\ 0 \\ 0 \\ 0 \\ 0 \end{bmatrix}$$

Equations (3.2.3) and (3.2.4) are now characterized with the exception of the weighting terms. Constants are used for both the output W and control $\overline{R}$ weighting matrices.

$$W = \begin{bmatrix} 4 & & & & & & & & & & & \\ & 5 & & & & & & & & & & \\ & & 15 & & & & & & & & & \\ & & & 70 & & & & & & & & \\ & & & & 0.8 & & & & & & & \\ & & & & & \ddots & & & & & & \\ & & & & & & 4 & & & & & \\ & & & & & & & 5 & & & & \\ & & & & & & & & 15 & & & \\ & & & & & & & & & 70 & & \\ & & & & & & & & & & 0.8 \end{bmatrix} \in \mathbb{R}^{250\times 250}$$

and

$$\overline{R} = \begin{bmatrix} 100 & & & & \\ & 100 & & & \\ & & \ddots & & \\ & & & 100 & \\ & & & & 100 \end{bmatrix} \in \mathbb{R}^{24\times 24}$$

such that the weights corresponding to each of the variables are identified as follows:

$$\begin{bmatrix} W_{\Delta u} \\ W_w \\ W_q \\ W_{\Delta\theta} \\ W_h \end{bmatrix} = \begin{bmatrix} 4 \\ 5 \\ 15 \\ 70 \\ 0.8 \end{bmatrix}, \begin{bmatrix} \overline{R}_{\delta_e} \\ \overline{R}_{\delta_t} \end{bmatrix} = \begin{bmatrix} 100 \\ 100 \end{bmatrix}$$

The controlled response of the aircraft, Figure 4.2, is no longer oscillatory. The altitude signal has a settling times of 6.9 seconds. The reduction to this value (from 25.1 seconds) comes at a cost of a 24% overshoot in speed, although significantly smaller than the previous 60%.

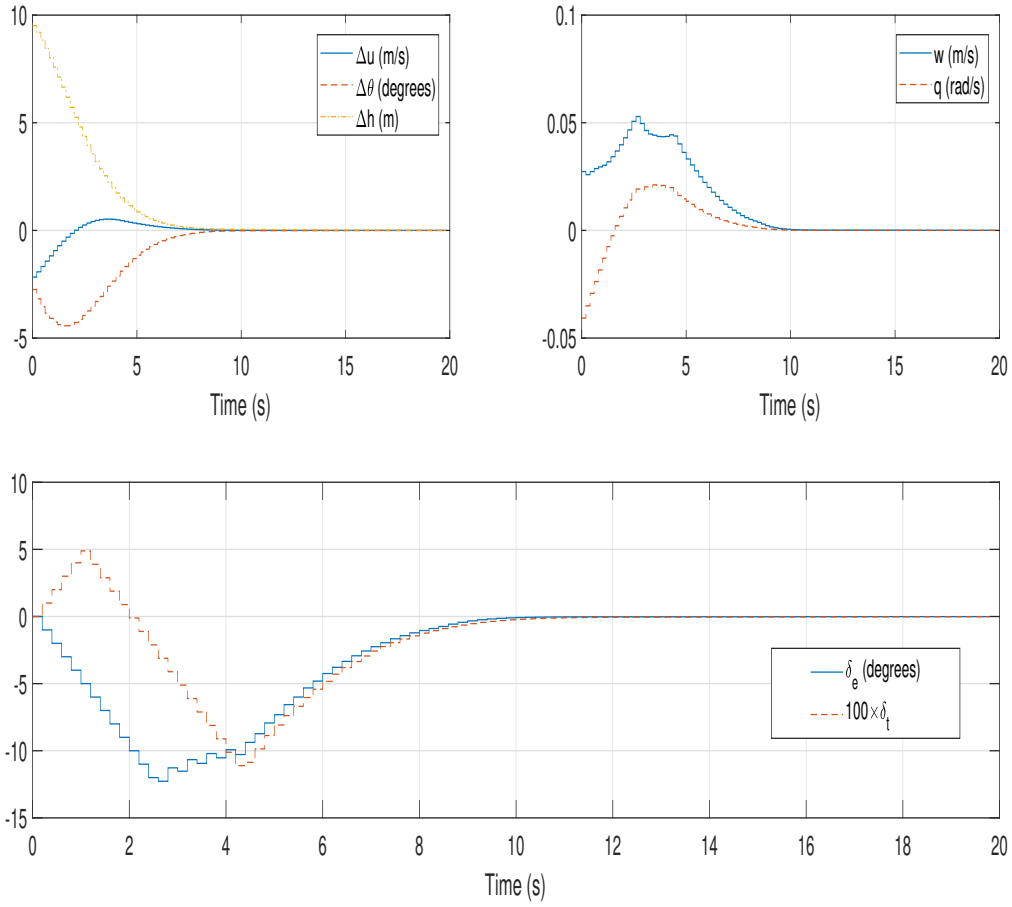

Figure 4.2: Phugoid Suppression

This performance is achieved by an elevon deflection (positive trailing edge down) to increase the pitch rate to reduce the negative climb angle and avoid an overshoot in terms of altitude. The throttle seems to be in charge of the forward speed, providing an acceleration for a brief period of time at the initial instants, followed by a reduction of the demand. This reduction is also linked to the speed increase that results of the altitude loss.

The final change of curvature of the two control laws happens earlier for the elevons than for the throttle, although in both cases with an anticipation of the order of one to two thirds of the settling time, allowing for a smooth transition to equilibrium.

The step-like appearance of the signal is used to represent the discrete time nature of the controller. For the sake of clarity, future Figures will be represented as continuous signals.

4.1.2 Spiral Suppression

The lateral spiral mode was shown to be unstable on Subsection 2.4.2. A controller with the following characteristics is built to restore the aircraft to equilibrium when

a disturbance excites this unstable mode:

- Sampling rate $\Delta t = 0.2$ seconds.
- Prediction horizon $N_p = 150$.
- Control horizon $N_c = 8$.

Similarly to the longitudinal dynamics, an augmented lateral system is built, by adding the kinematic variable ψ, given by Equation (2.1.12), to the lateral Equations of Motion (2.1.11).

The output is selected equal to the state vector ($C = I_{5\times5}$). The weights assigned to each of the outputs and to the control are as follows:

$$\begin{bmatrix} W_v \\ W_p \\ W_r \\ W_\phi \\ W_\Psi \end{bmatrix} = \begin{bmatrix} 1 \\ 1 \\ 1 \\ 1 \\ 1 \end{bmatrix}, \overline{R}_{\delta_e} = 1$$

The evolution of the heading angle on Figure 4.3 shows a slow return to the reference value. This is indicative of a poor lateral manoeuvrability. This result has been confirmed by Wake Engineering in a vis-a-vis meeting.

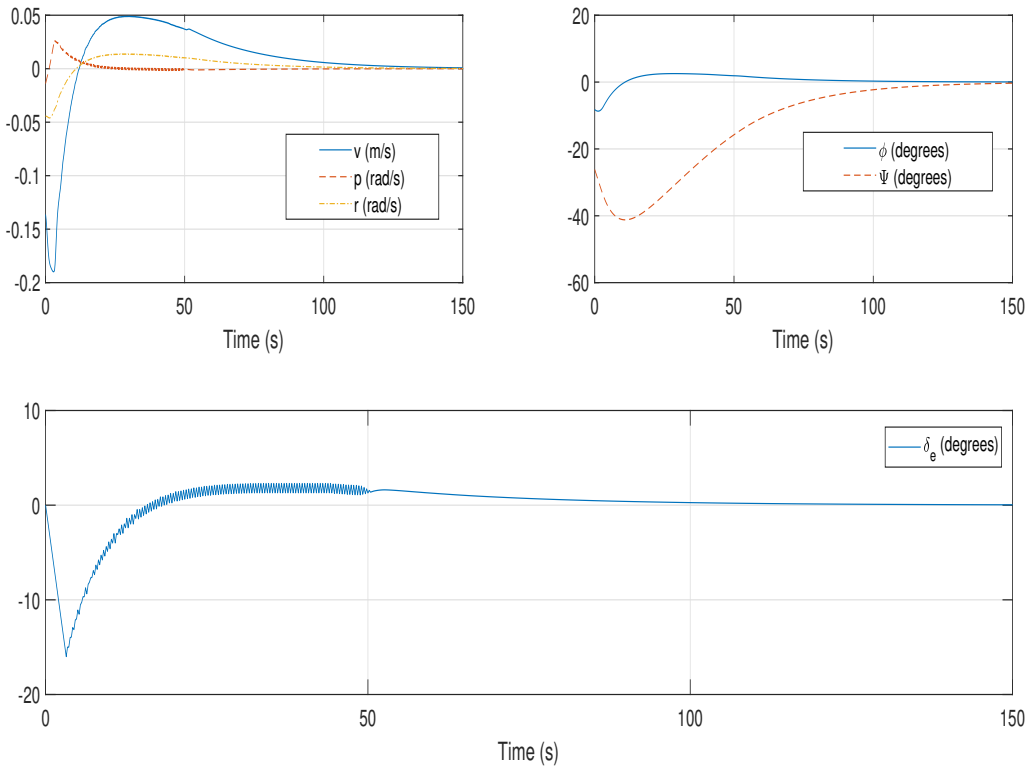

Figure 4.3: Spiral suppression. $N_p = 150$. $N_c = 8$.

In fact, measuring the lateral control capabilities in terms of the control derivatives of the lateral actuation of the elevons, these fall one order of magnitude below its longitudinal counterparts. Particularly, the ability of the elevons to produce a yawing moment is significantly limited. This is traced back to the fact that the elevons (the only deflectable surface) are placed on the wing. Therefore, the contribution of the deflection of the elevons to the yawing moment of the aircraft can be approximated by the increase in drag associated to it (which multiplied by the moment arm produces the yawing moment). By establishing a lift to drag ratio associated to the deflection of the elevons of an order of magnitude of 10, the difference between longitudinal and lateral control capabilities could be justified.

The low control capabilities, together with the large prediction horizon, $N_p = 150$, constrain a small positive elevon deflection for a long time period, ensuing no overshoot in the heading. As a consequence, the signals settles at a time of 121 seconds.

The observable oscillations of the control, which also the roll rate p experiences, are found to be difficult to smooth with the tuning of the available control parameters. An increase of the control weights certainly avoids the excessive oscillation of the controls, but comes at a cost of a much slower response. Bearing in mind the presence of an unstable mode, the controller needs to assure a response faster than the characteristic speed of the spiral mode.

The control instabilities are attributed to the presence of a sole lateral control, which could face a conflict to satisfy simultaneously two or more independent variables, resulting in an alternative variable targeting sequence of controls.

To explore the effect of the prediction horizon, it is set to $N_p = 40$, while keeping the rest of the control parameters constant.

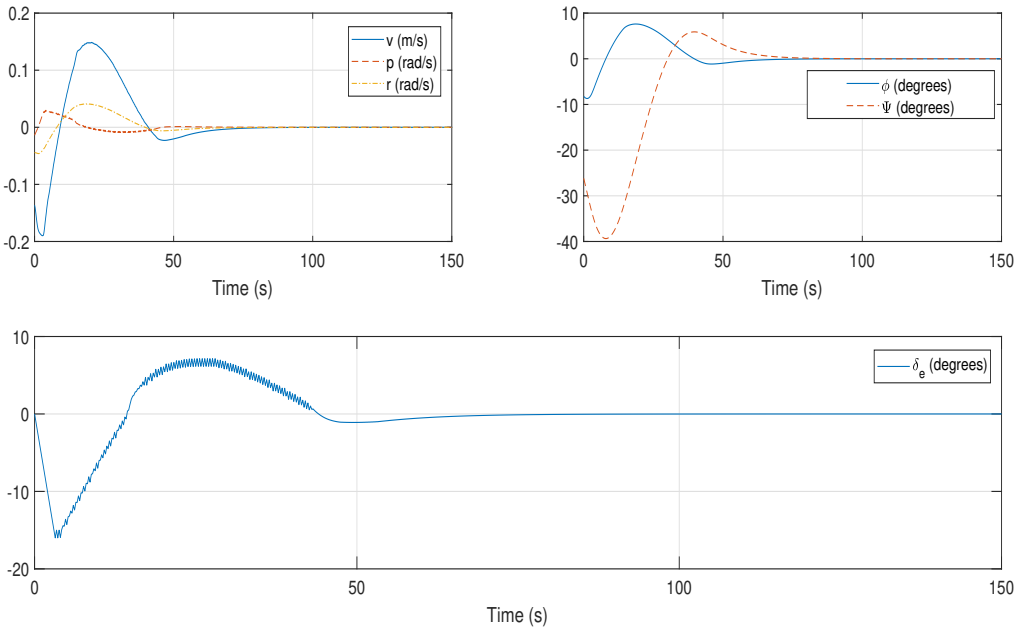

Figure 4.4: Spiral suppression. $N_p = 40$. $N_c = 8$.

A more aggressive controller is obtained, with the settling time being reduced to 63 seconds, but with an overshoot of 15%. The prediction horizon N_p is therefore an indicative of how further ahead of the current time instant the deviations of the output from the reference signal are significant to the optimization problem. However, the size of such problem is not determined by the dimensions of the prediction equation.

Recalling Equations (3.2.3) and (3.2.3), the size of the quadratic programming problem is determined by the control horizon, N_c, and the number of controls, m.

For a given prediction horizon N_p, the output of the optimization problem produces a control law that is a sequence of N_c control actions. In other words, the optimal control law to minimize the discrepancy between the predicted output and the future reference signal, is spread throughout N_c actions. Therefore, by introducing a smaller control horizon, the control law condenses in a shorter sequence the total control effort. This does not necessarily imply a more aggressive control, as is exemplified in Figure 4.5:

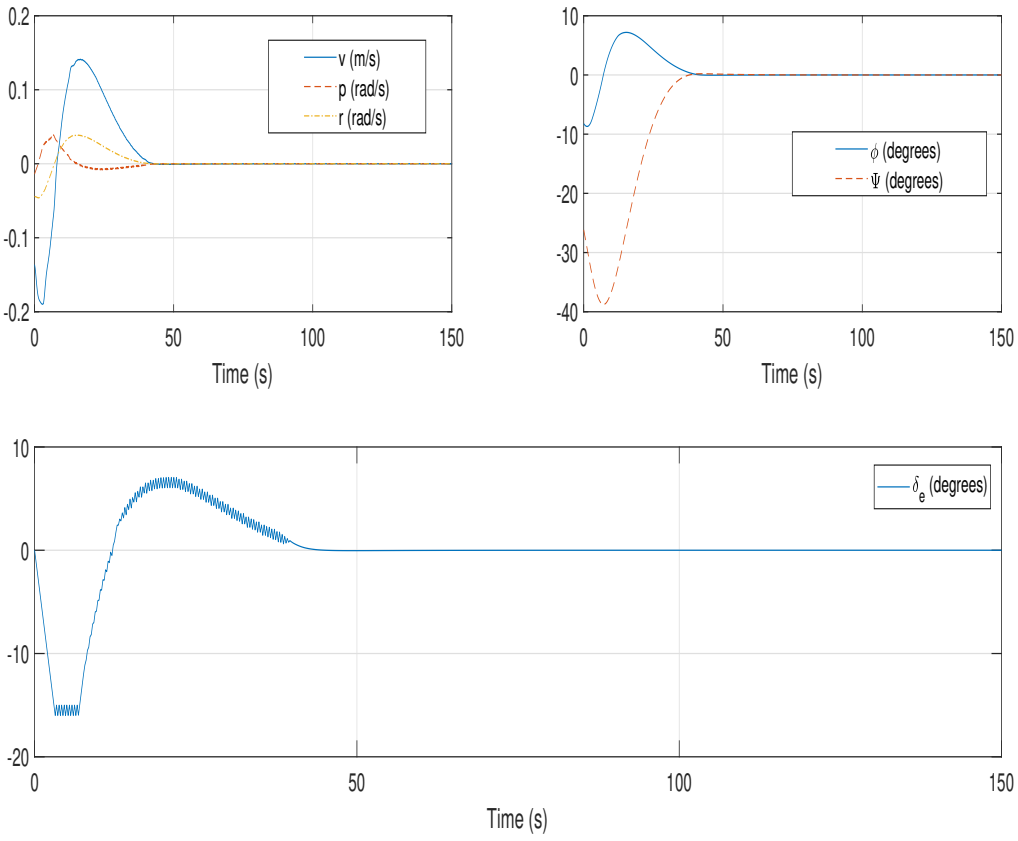

Figure 4.5: Spiral suppression. $N_p = 40$. $N_c = 4$.

An improvement with respect to Figure 4.4 in terms of overshoot (barely any) and settling time (34 seconds) is observed, by setting the control horizon $N_C = 4$. What is more, the computational load of the controller is reduced, due to the reduction in size of the optimization problem.

The difference in the evolution of the control between these two figures resides

in the following. For the case of $N_c = 8$, the control signal turns negative at the end to compensate the overshoot. However, the control signal corresponding to $N_c = 4$ remains for a longer time oscillating between -15 and -16 degrees at the initial instants, instead of performing corrective effort at the end.

4.2 Manoeuvres

The manoeuvres described hereafter serve as a preface to the simulation of a complete flight mission. At every time instant, the dynamics of the aircraft are interpolated in terms of speed and altitude. This raises a series of implications concerning the longitudinal dynamics.

Firstly, the interpolated dynamics correspond to the linearization about the current forward speed u. Such forward speed is the addition of the previous reference speed, u_0, and the most recent Δu. As a consequence, the state variable Δu needs to be set equal to zero at the beginning of each optimization problem. This in turn requires the reference signal to be adjusted consequently, as it provides a reference value for Δu, not for the absolute forward speed.

Secondly, the altitude, which enters into the dynamics through the density, is also part of the interpolation. However, it is merely a kinematic variable, which does not determine the evolution in time of the other variables (the last column of the augmented longitudinal state matrix A is a column of zeros). Therefore, it is not necessary to set Δh equal to zero.

Finally, the other state variable with a reference condition that need not be zero, is the pitch angle. Unlike in the case of the forward speed, this term is not set to zero at the beginning of each iteration. This is because the pitch angle, θ, is not a variable of interpolation. The mesh in terms of speed and altitude was generated for a reference value θ_0 equal to zero. This means that the deviation from θ_0, measured by $\Delta\theta$ is equally applicable to any combination of speed and altitude.

For future reference, the function that determines the current dynamics, could be programmed to take as input the current pitch angle, prior to the interpolation in speed and altitude. The benefits would depend on the range of variation of the aircraft's pitch.

4.2.1 Change in speed

This manoeuvre is defined as a transition to a different cruising speed, while keeping the same flight level.

The controller is designed with the following parameters:

- $\Delta t = 1$ second.
- $N_p = 40$.
- $N_c = 4$.

The strategy is to target three state variables, the forward speed, the pitch rate, and the height, so that the output matrix is defined as:

$$C = \begin{bmatrix} 1 & 0 & 0 & 0 & 0 \\ 0 & 0 & 1 & 0 & 0 \\ 0 & 0 & 0 & 0 & 1 \end{bmatrix}$$

Regarding the weights, exponential weighting is introduced for the speed and for the height. In terms of the coefficient α defined in Subsection 3.2.1:

$$\alpha_{\Delta u} = 1.21$$
$$\alpha_{\Delta h} = 1.01$$

The objective of this decision is to prioritize the acquisition of the new cruising speed at the early instants, while considering of equal importance the achievement of the reference height at the end of the prediction horizon, where both weighting terms become equal to 1.

Regarding the pitch rate, it is incorporated in the control problem to avoid attitude oscillations after the attainment of the final speed and height. It has a null reference signal throughout the whole manoeuvre, and a constant weighting term equal to $W_q = 10^8$.

Finally, the control weights: $\overline{R}_{\delta_e} = 1500 = \overline{R}_{\delta_t}$.

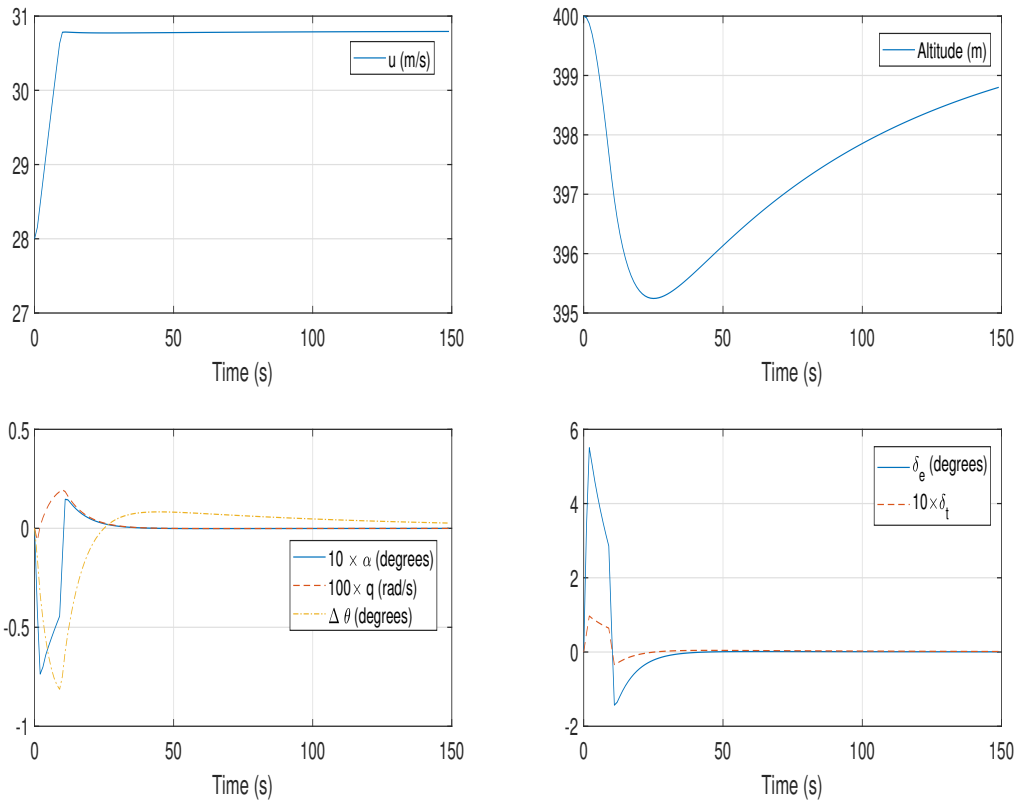

Figure 4.6: Manoeuvre: change of speed.

Figure 4.6 shows the response to achieve a 10% change in cruising speed.

The speed signal has a settling time of 9.5 seconds. Furthermore, it is achieved with no overshoot, and a steady state error smaller than 0.01%. To achieve this behaviour, a pitch down motion results in a change of altitude of 4.7 metres, less than 15 feet, accelerating the aircraft. The recovery from this value to the nominal cruise altitude is significantly slow, as a consequence of the tight control of the speed. However, the magnitude of this variation is considered not to be concerning.

4.2.2 Change in altitude

The controller designed to manage a change in altitude adopts the same parameters as the previous, for the exception of the weights of altitude and speed:

$$\alpha_{\Delta u} = 1.20$$
$$\alpha_{\Delta h} = 1.12$$

The sample manoeuvre considers a change in altitude of 50 metres. The response is shown in Figure 4.7 below:

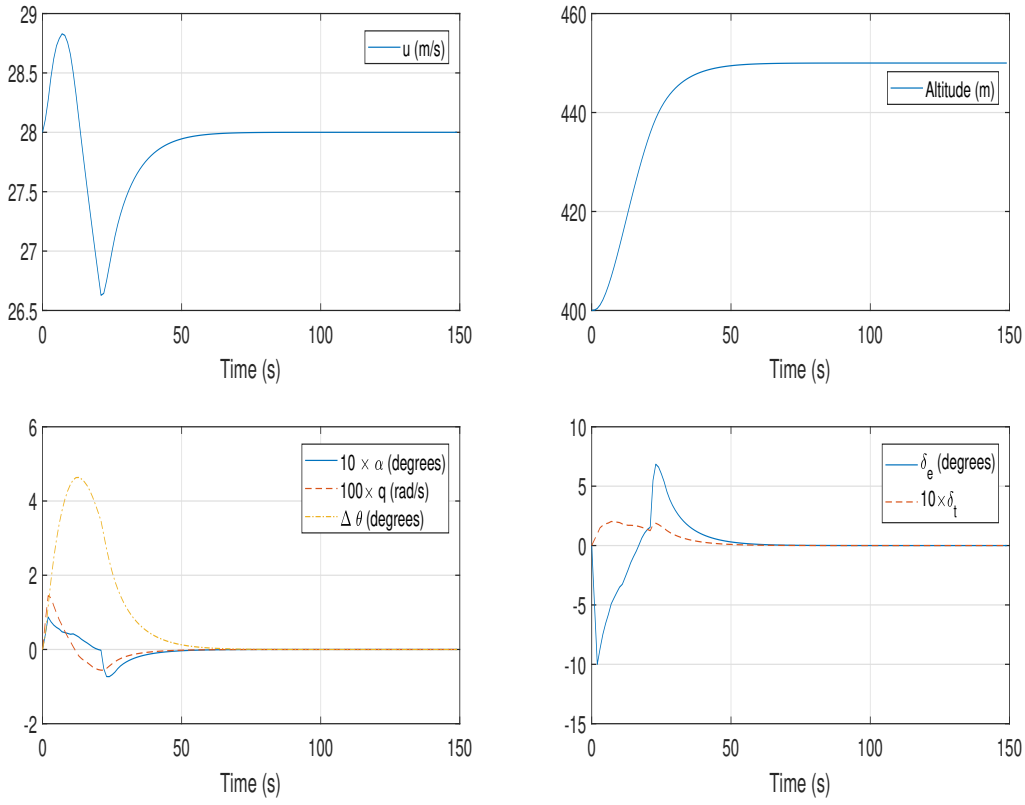

Figure 4.7: Manoeuvre: change of altitude.

Opposite to the behaviour presented in the speed controller, this response is more lenient with the variations of the speed to allow for a faster altitude adaptation, particularly a settling time of 44.5 seconds, corresponding to a climb rate of 221 fps; and null overshoot and steady state error.

The speed variations are contained within ± 1.5 m/s of the reference cruise speed, and a settling time of the order of that of the altitude.

It should be noted that the coefficients of the exponential weights for the speed and altitude follow the same tendency than in the speed controller. Meaning that the coefficient for the speed is also greater than for the altitude, instead of selecting a higher coefficient for the altitude output in the altitude controller. This is the result of the need to impose a tighter control on the speed, given the low order of magnitude of the range of working dynamic pressures.

4.2.3 Change in heading

The ability to select a given heading is the only selected lateral manoeuvre, as a mean to perform a turn. The control parameters are the following:

- $\Delta t = 1$ second.
- $N_p = 40$.
- $N_c = 4$.

The approach to control the manoeuvre is similar to the suppression of the spiral mode. The complete lateral state vector is selected as output, meaning that $C = I_{5\times 5}$.

Exponential weighting is also introduced, with the same coefficient for each of the lateral variables: $\alpha = 1.5$. Therefore, all variables are given equal consideration, but the control law is set to favour initial differences with the reference signal. The weight on the control is constant, such that $\overline{R}_{\delta e} = 0.1$.

Figure 4.8 below shows the response of the aircraft to a commanded heading angle of 30°.

The transition to the new heading settles after 33.6 seconds, with no overshoot and a steady state error below 0.01%. The average turn rate corresponds to 1.12 degrees/s, peaking at a maximum yaw rate $r = 2.29$ degrees/s.

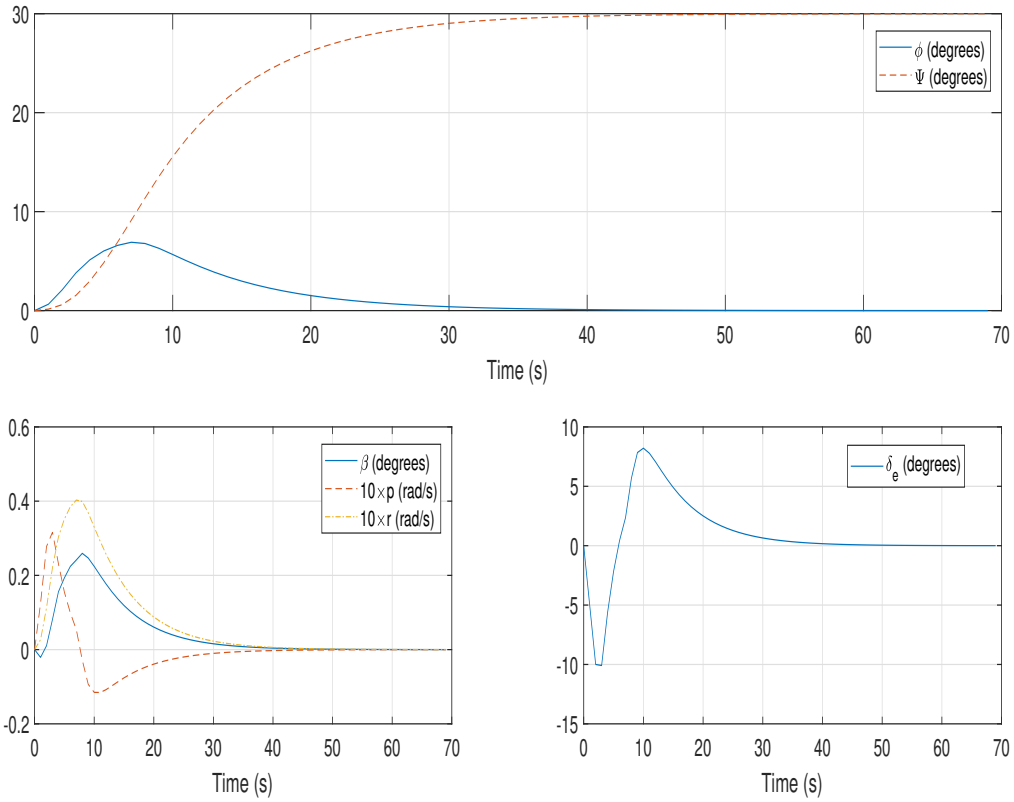

Figure 4.8: Manoeuvre: Change of heading.

Chapter 5

MPC flight mission simulation

In this chapter, the results of previous section are put together to develop a controller for a complete flight mission.

5.1 Previous considerations

In a given flight mission, there is a need to monitor both the longitudinal and lateral dynamics of the aircraft. This can be achieved by introducing two independent control units. Another possibility is to share a single set of resources, which seems reasonable given the weight and space specifications of the Fulmar.

Therefore, a single controller, that deals simultaneously with both the longitudinal and lateral dynamics is developed. A single 10-by-10 state matrix A is built, where each of the original matrices occupy the first and last five rows and columns respectively, with the rest of the entries equal to zero. Similarly, a 10-by-3 matrix of controls is built. The first five rows and two columns are reserved for the longitudinal controls, and the last five rows, and third column, for the lateral control.

This single formulation maintains the uncoupling of the two dynamics, and allows to pose a single quadratic programming problem, which however does introduce a fictitious coupling between the two different set of controls. This is a consequence of the nature of the cost function. The cost function is a scalar, which the output of the optimization problem is set to minimize. Ultimately, the value of the cost function results from the addition of the three different controls, scaled by terms coming from the propagation of the dynamics, and from the selected weights.

Therefore, a single formulation to deal with the two dynamics at the same time might raise a series of issues. Particularly if it is desired to perform at the same time a longitudinal and lateral manoeuvre. Most likely, this is not a required capability of the Fulmar. Therefore, manoeuvres are designed to happen sequentially.

However, this arrangement of the different manoeuvres alone does not guarantee that the aforementioned fictitious coupling disappears. It is also necessary to resort

to the mesh defined in Subsection 2.3.2.

The use of constant state and control matrices defined for a given reference cruise condition implies that in order to transition to a different equilibrium, for instance, at a different speed, the steady state value of the terms Δu, and most importantly, of the controls δ_e and δ_t are different than zero. However, by considering a variable description of the system dynamics, the steady state value of these terms, in the context of linear theory, is equal to zero.

This is important due to the following: consider a steady state value of the longitudinal controls different than zero. If a lateral manoeuvre is to be initiated, the output of the optimization problem is seen to involve the actuation of the longitudinal controls to favour the lateral manoeuvre. As a consequence, oscillations occur in the longitudinal variables. To illustrate this feature, Figure 5.1 shows a segment of a flight mission, in which a heading change is initiated, at a $\Delta u \neq 0$, with the corresponding oscillations, appreciable as well in the controls.

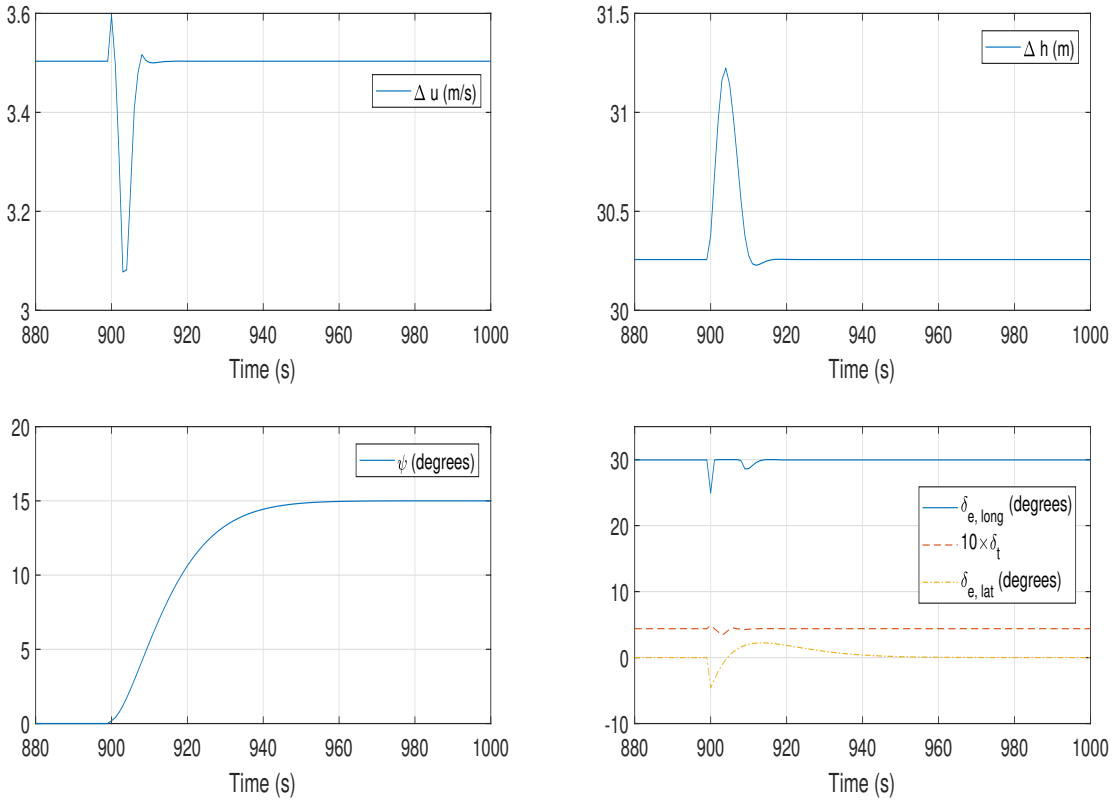

Figure 5.1: Longitudinal and lateral coupling

By making use at every instant of the linear dynamics corresponding to the aircraft's forward speed u, this issue is resolved.

5.2 Control structure

The approach to the design of the controller is to define different modules. Each module is in charge of monitoring a particular manoeuvre.

According to this reasoning, any given flight mission is divided into segments. To each of this segments, a particular module is assigned. Similarly, the reference signal needs to be properly configured for each segment, as the dimension of the output vector y might change from one module to another.

Building on top of Chapter 4, a total of four modules are defined, which share the following parameters:

- $\Delta t = 1$ second.
- $N_p = 40$.
- $N_c = 4$.

Stability Module

Every longitudinal and lateral variable is held at the reference cruise value. Therefore, the observation matrix corresponds to $C = I_{10\times10}$.

Regarding the weights, constant weighting is employed, equal to 1000 for each of the state variables, enough to inhibit the spiral mode. The control weights correspond to $\overline{R}_{\delta_{e,long}} = 1500$, $\overline{R}_{\delta_t} = 1500$, $\overline{R}_{\delta_{e,lat}} = 0.1$.

Speed Change Module

Defined for changes in cruise speed. The lateral variables are held constant, inhibiting the expression of the spiral mode. The observation matrix is defined as follows:

$$C = \begin{bmatrix} 1 & 0 & 0 & 0 & 0 & \\ 0 & 0 & 1 & 0 & 0 & \\ 0 & 0 & 0 & 0 & 1 & \\ & & & & & I_{5\times5} \end{bmatrix}$$

Exponential weighting is used for the output variables, with the exception of the pitch rate. The corresponding coefficients for the exponential weights, and the constant term for the pitch rate are the following:

$$\begin{aligned} \alpha_{\Delta u} &= 1.21 \\ W_q &= 10^8 \\ \alpha_{\Delta h} &= 1.01 \\ \alpha_{lat} &= 1.30 \end{aligned}$$

where the same coefficient is used for every lateral variable.

The coefficient used for the lateral variables is relatively severe. However, in the case that a longitudinal manoeuvre is initiated prior to the conclusion of a lateral one, this weighting also allows for a smooth transition of the lateral variables to their reference state.

The control weights employed are equal to those of the stability module.

Altitude change module

Defined for changes in cruise altitude. The lateral variables are held constant, inhibiting the expression of the spiral mode. The observation matrix is identical to the speed change module.

Output weights:

$$\begin{aligned} \alpha_{\Delta u} &= 1.20 \\ W_q &= 10^8 \\ \alpha_{\Delta h} &= 1.12 \\ \alpha_{lat} &= 1.30 \end{aligned}$$

Control weights are equal to those in the stability module.

Heading change module

Defined for changes in heading. The longitudinal variables are held constant. The observation matrix is identical to the employed in the speed change module.

Output weights:

$$\begin{aligned} \alpha_{\Delta u} &= 1.15 \\ W_q &= 10^8 \\ \alpha_{\Delta h} &= 1.12 \\ \alpha_{lat} &= 1.30 \end{aligned}$$

The control weights are equal to those in the stability module.

5.3 Flight Mission Simulation

To test the performance of this controller in a representative area of the envelope generated in Subsection 2.3.2, the following flight mission is designed:

1. Starting from a cruise at 28 m/s and 400 metres in altitude, a 10% speed increase at constant altitude is performed at $t = 20$ seconds.
2. At $t = 350$ seconds, a change in altitude of 35 metres, or 115 feet, is performed, at constant speed.
3. At $t = 550$ seconds, the speed is reduced to 5% above the initial reference speed to 29.4 m/s, holding the altitude.

4. At $t = 1150$ seconds, the aircraft's heading is changed by 15°.

5. In order to simulate an approach manoeuvre, a series of changes in altitude followed by changes in speed are performed:

   (a) At $t = 1300$ seconds, descend to 265 metres, followed at $t = 1950$ seconds by a speed reduction to 28 m/s.

   (b) At $t = 2150$ seconds, descend to 165 metres, followed at $t = 2700$ seconds by a 10% speed decrease, to 25.2 m/s.

   (c) At $t = 2800$ seconds, final descend to 50 metres, followed at $t = 3300$ seconds by a speed decrease to 21 m/s.

The results of the whole simulation are shown in Figures 5.2 and 5.3.

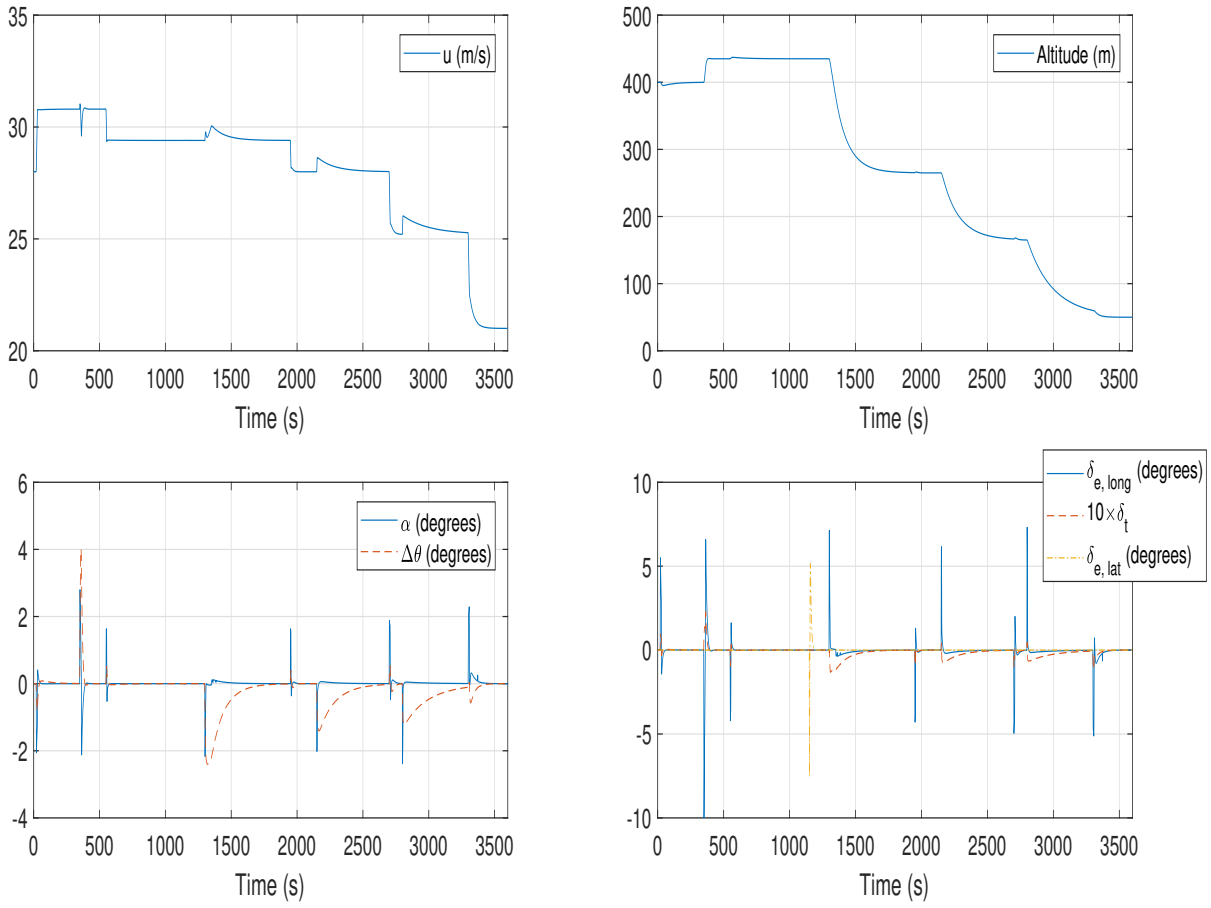

Figure 5.2: Flight mission: longitudinal dynamics and controls

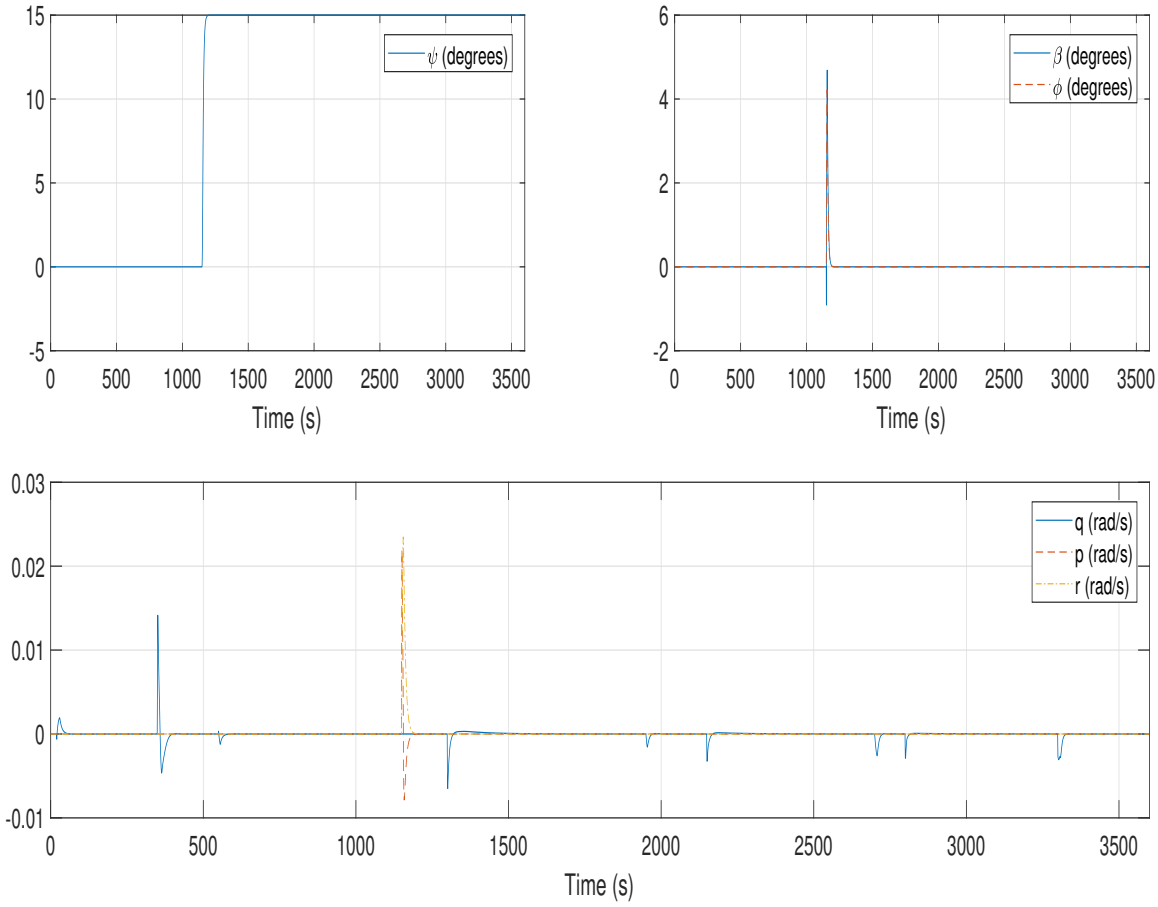

Figure 5.3: Flight mission: lateral dynamics

The performance of the controller is now evaluated individually for each of the segments.

The first speed increase, shown in Figure 5.4, has a settling time of 9.5 seconds. The manoeuvre is performed with null overshoot, and a steady state error smaller than 0.01%. There is a loss in altitude smaller than 5 metres that is slowly recovered.

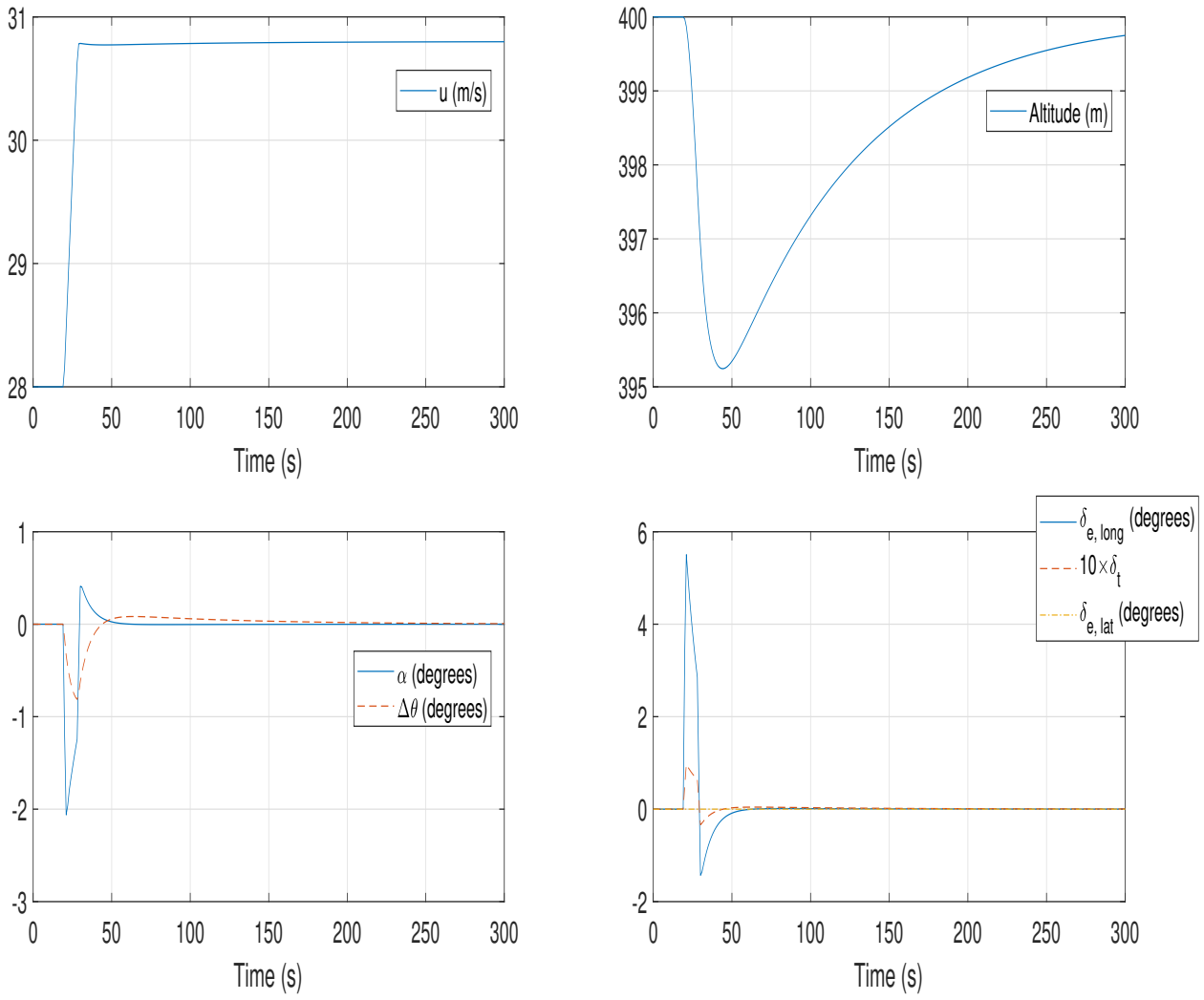

Figure 5.4: First segment of the mission

The second segment, Figure 5.5, includes the climb to 435 metres. Such manoeuvre has a settling time of 27.9 seconds. This is equivalent to an average climb rate of 247 feet per minute. It is performed with a 1.26% of overshoot, and a not appreciable steady state error. To achieve this new altitude, an oscillation of 1.5 m/s affects the forward speed. In this segment, the highest increase in value of angle of attack is reached, a total of +2.8°. Given that the aircraft is operating close to its nominal specifications, the appearance of this transient value is not considered to be a severe aerodynamic issue.

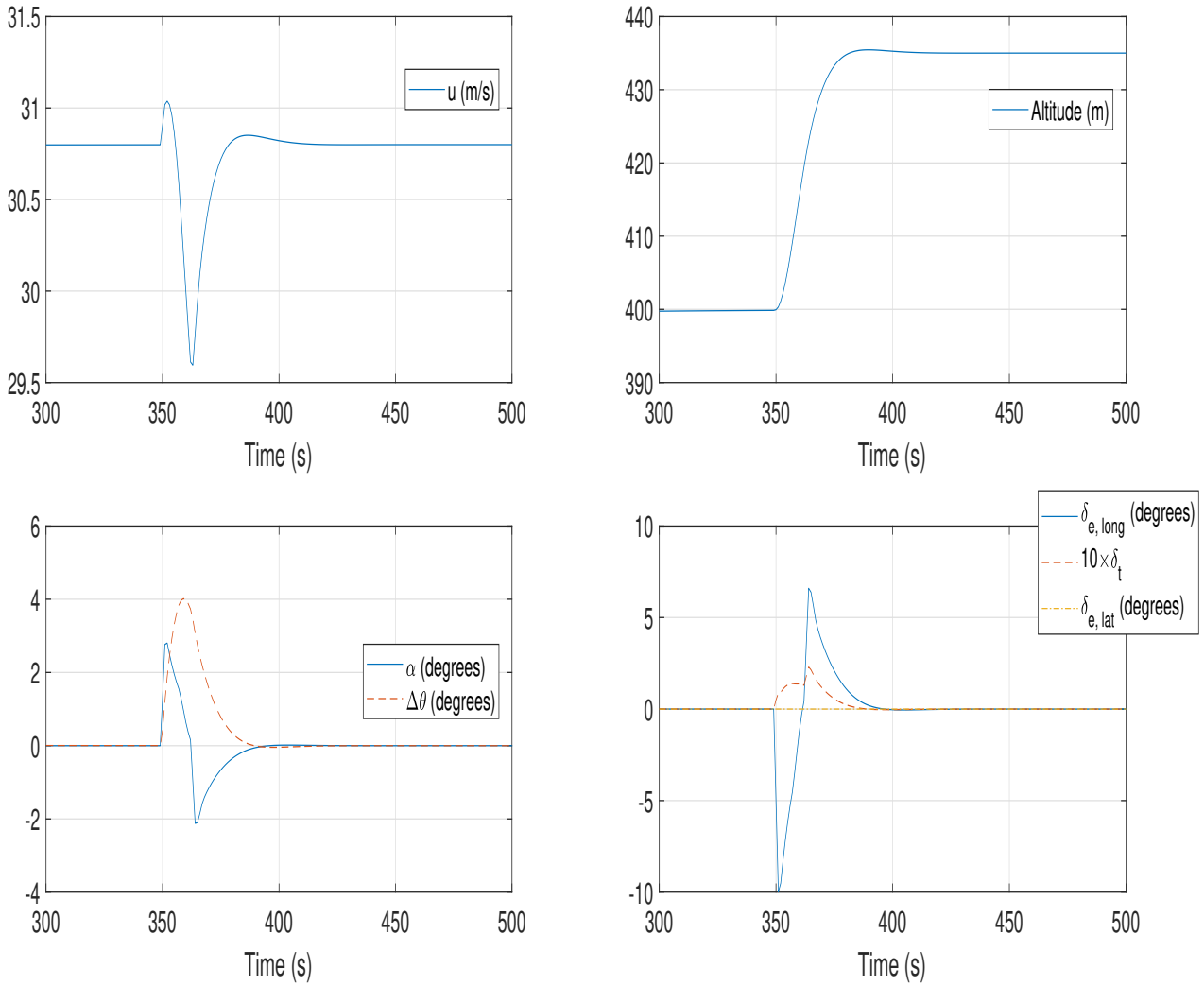

Figure 5.5: Second segment of the mission

The reduction to 29.4 m/s of speed during the third segment is shown in Figure 5.6. The signal settles in 7.4 seconds, with a 1.26% overshoot, and with a steady state error smaller than 0.001%.

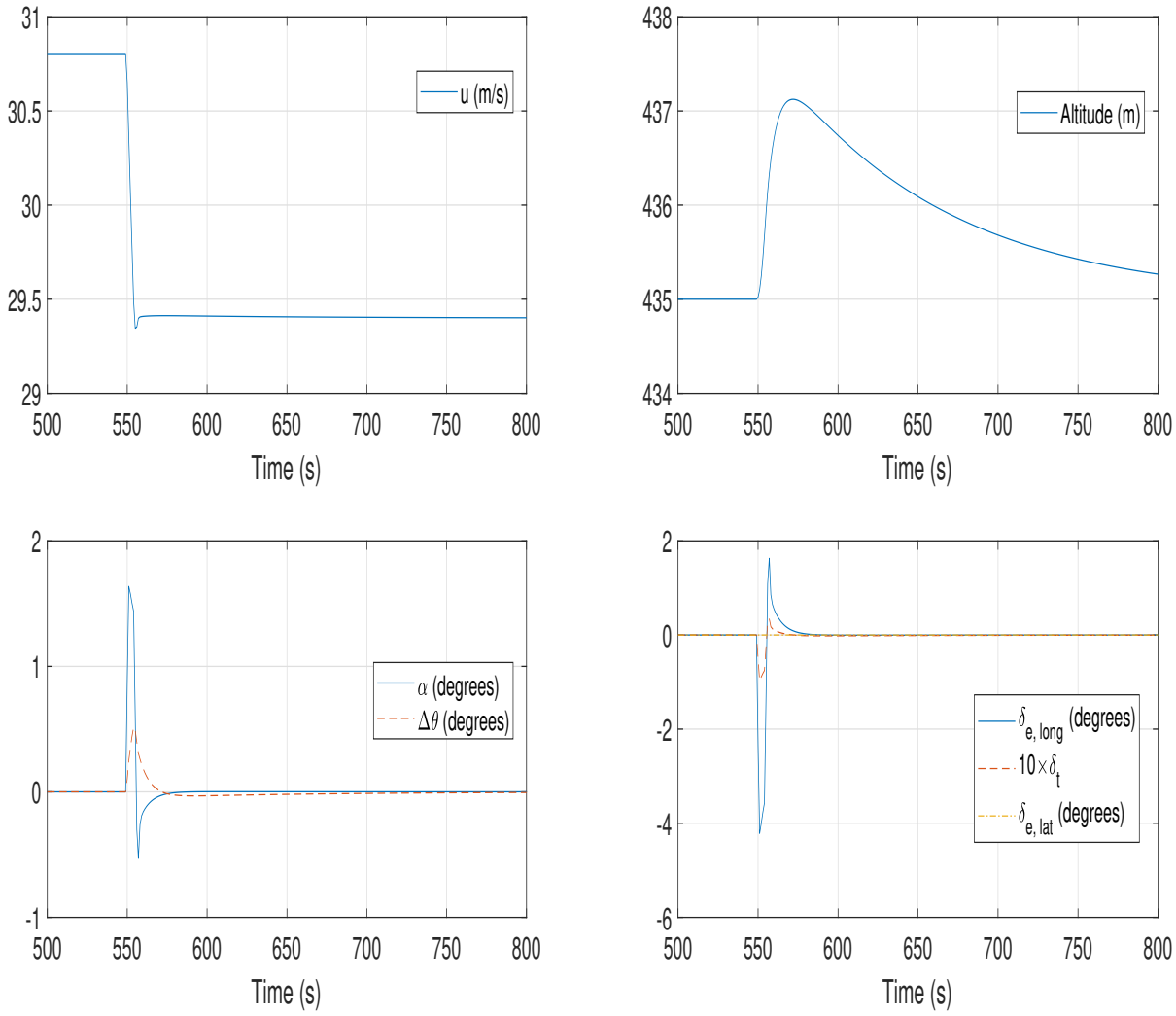

Figure 5.6: Third segment of the mission

The segment prior to the descend is the change of heading, corresponding to 15°. Figure 5.7 represents the lateral dynamics of this manoeuvre. A settling time of 27 seconds, related to an average turn rate of 0.556 degrees/s, with null overshoot, and a non-appreciable steady state error.

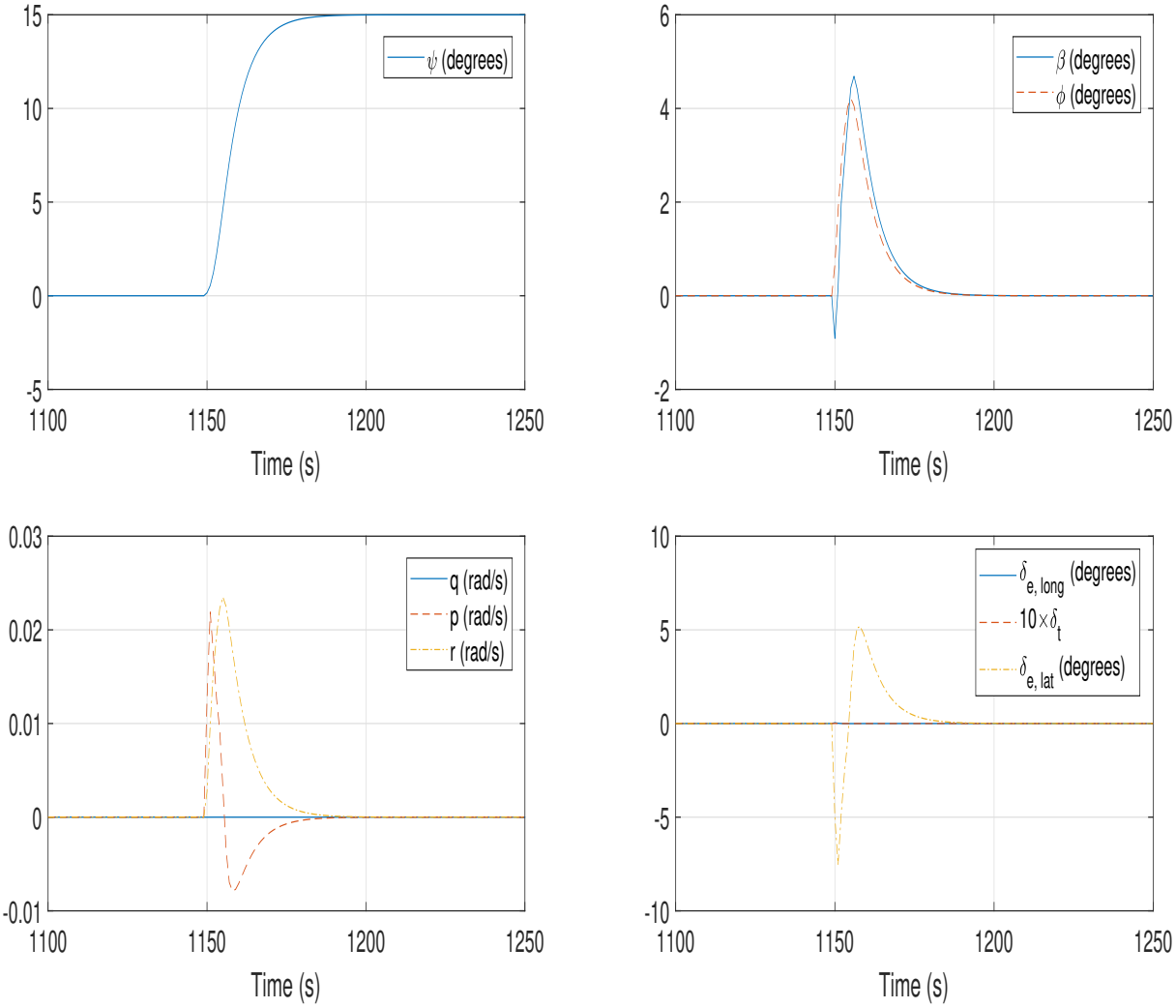

Figure 5.7: Fourth segment of the mission

Finally, the performance of the controller during the descend is shown in Figure 5.8. In spite of a transient peak of $-2.4°$of angle of attack, the absence of overshoot

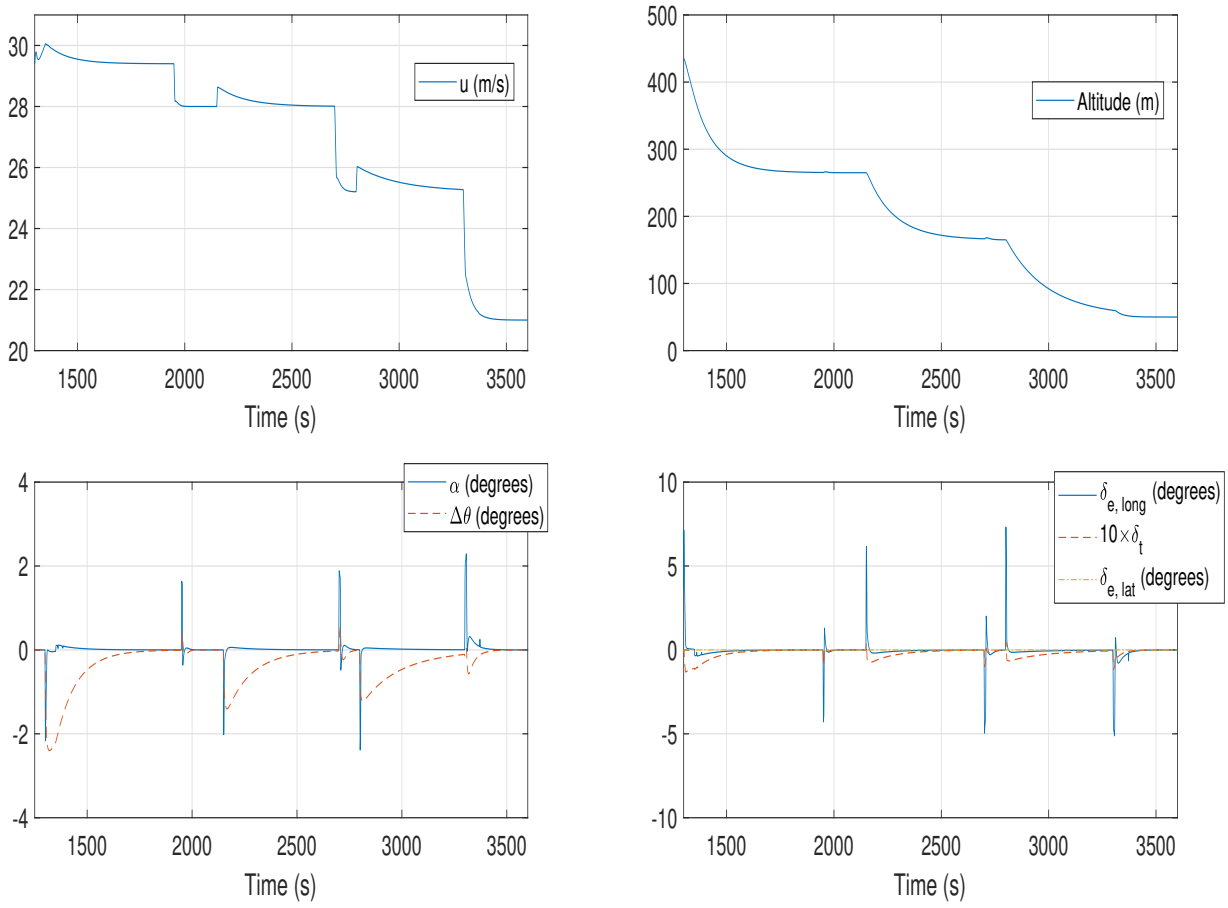

Figure 5.8: Descend segment of the mission

both in altitude and speed decrease during the descend segment is a positive feature, bearing in mind that the aircraft is progressively operating closer to the stall region. In fact, engineers from Wake Engineering indicate that the ability to control the speed during the landing phase is one of the major concerns that this particular aircraft faces. These results are gathered in table 5.1 below.

Descend Segment	Settling time (s)	Overshoot (%)	Steady State Error (%)
5a Altitude	406.9	0	$< 0.001\%$
5a Speed	34.6	0	$< 0.001\%$
5b Altitude	111.9	0	$< 0.24\%$
5b Speed	7.7	0	$< 0.02\%$
5c Altitude	560	0	$< 0.28\%$
5c Speed	107.5	0	$< 0.01\%$

Table 5.1: Descend performance

As a closing note, in order to get a taste of the computational load associated to the implementation of this particular control scheme, the time to run this complete simulation in a 2.40 GHz computer is given. This number is seen to vary between 8.5 and 12.5 seconds. A complete simulation of this 3600 seconds long mission consists on the resolution of 3600 optimization problems. The output of each optimization problem is a vector in $\mathbb{R}^{12}$, equal to the product of the number of controls (3) and the control horizon (4).

Chapter 6

Conclusions and Future Work

6.1 Conclusions

The advent of Unmanned Aerial Vehicle civil and military applications involves the development of sophisticated control schemes that are able to satisfactorily deal with these multivariable processes.

The foundations for the development of a Model Predictive Control autopilot for the mini-UAV Fulmar X have been laid. An analysis of the dynamics of the aircraft has indicated the presence of oscillatory aircraft modes, as well as the presence of a divergent spiral mode. Furthermore, the PID controller that the aircraft currently incorporates is known to poorly operate in the approach and landing segment, with a loose control of the aircraft's speed, in danger of stall.

The proposed solution defines several modules, each of which is designed to manage a given functionality of the aircraft: maintain stable cruise and the ability to change altitude, speed or heading.

The results show that the controller performs adequately throughout the Fulmar's flight envelope. In the descend and approach manoeuvre, the aircraft's speed is decreased without an overshoot that would compromise the controllability of the platform. Regarding the dynamic stability of the aircraft, the controller deals effectively with perturbations that excite oscillatory modes, as well as the unstable spiral mode. It is clear that signs of limited lateral manoeuvrability are present, confirmed by Wake Engineering engineers, attributed to the unconventional aircraft typology which includes one single lateral control.

6.2 Future Work

The degree of development of the project leaves open various research paths. Firstly, a refinement of the model for the aircraft dynamics through flight testing, including a detailed characterization of the aircraft controls, such as the dependence of thrust

with altitude and speed.

Secondly, Wake Engineering has shown interest in the development of a robust control strategy. For this purpose, Robust Model Predictive Control is an option to be explored, which accounts for uncertainty in the model for the aircraft dynamics in the optimization process. Such uncertainty is mainly due to the tolerance associated to the manufacturing process of each of the aircraft components.

Finally, concerning the strengthening of the current modular controller, it would be convenient to test the ability of each of the modules to deal with random disturbances that affect the state variables during the flight mission, in order to account for atmospheric phenomena. Another relevant aspect to consider is the introduction of constraints that would couple the amplitude of the longitudinal and lateral actuation of the elevons, which have been considered as indepented controls in this project.

Appendix

Appendix A

Phugoid Suppression: MPC vs LQR

The response of the MPC controller to a disturbance that excites the phugoid mode shown in Figure 4.2 is repeated below:

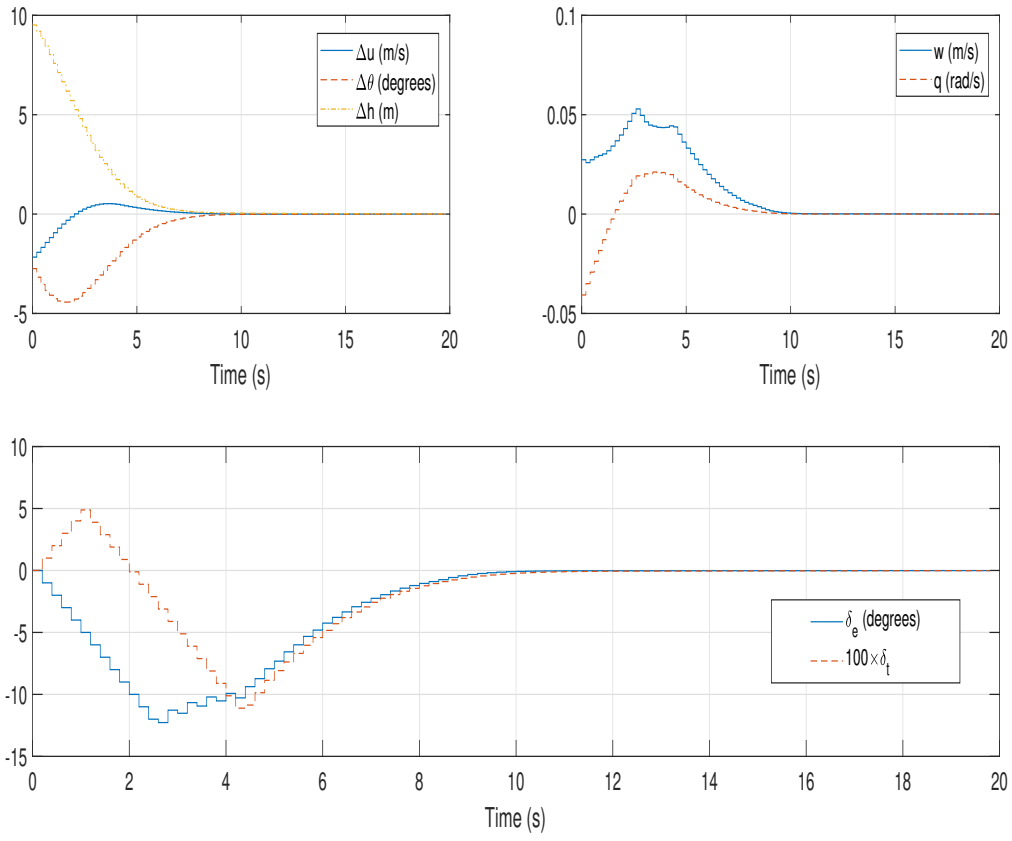

Figure 4.2: MPC phugoid suppression (repeated from page 32)

Alejandro Torres Gamiz, currently working on his Master's Thesis "Linear Quadratic Regulator Application to a Remotely Piloted Aircraft System (RPAS)'s Autopilot", has provided the response to the same disturbance generated by LQR control, shown in Figures A.2 for the state variables and A.3 for the controls:

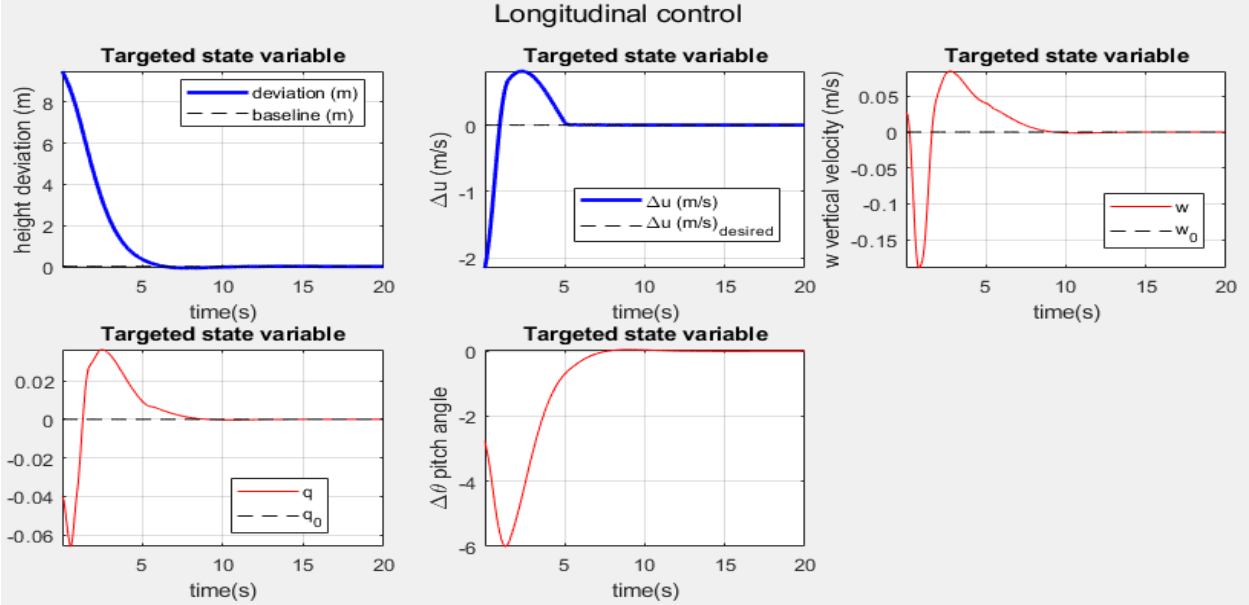

Figure A.2: LQR phugoid suppression: dynamics

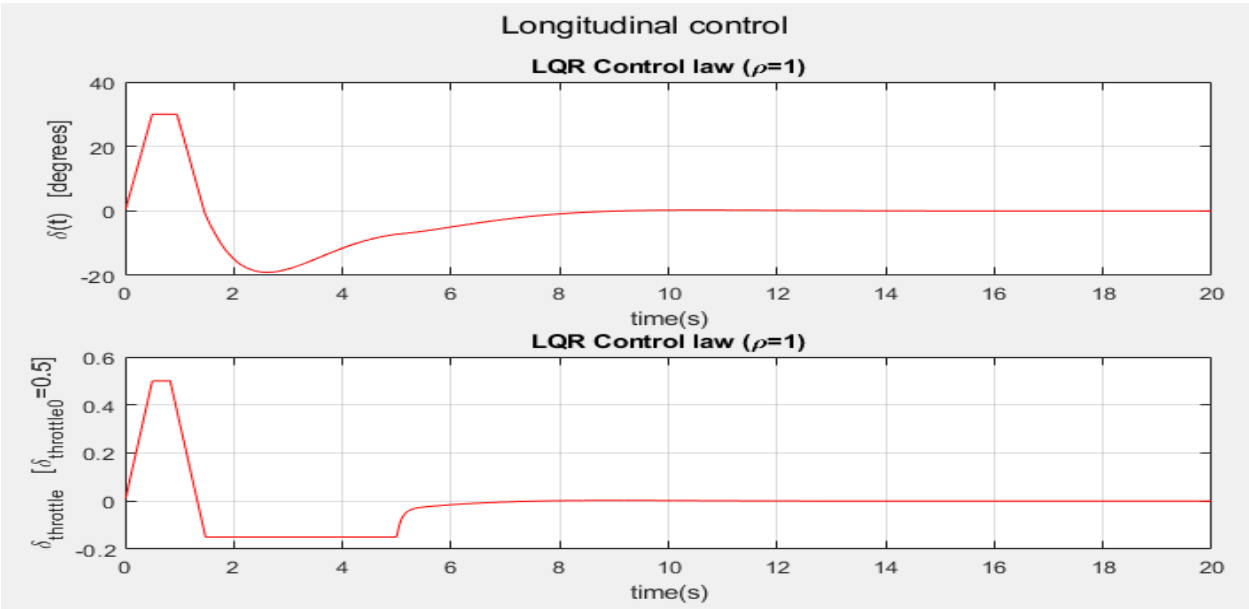

Figure A.3: LQR phugoid suppression: control

It should be noted that the rate constraints in the throttle are less restrictive in the LQR control. The response is still in the process to be refined. However, the tendency of each of the control schemes on how to suppress the disturbance is clearly exemplified.

The behaviour of the state variable signals is detailed in the following bullet points:

- The altitude signal returns to equilibrium without overshoot in both cases.
- Overshoot of the order of 40% to 50% in speed in LQR control, against a 24% in MPC.

The remaining state variables are easily understood by the comparison of the control law. The main difference is the deflection of the elevons. In the case of LQR, the elevons initially deflect to induce a pitch down motion, in order to both decrease the altitude and regain speed. Eventually, this deflection turns negative to compensate the overshoot in the speed. In the MPC response, however, the elevon's deflection is negative from the beginning, inducing a pitch up motion, that does not contribute to an acceleration. This is supported by the behaviour of the pitch rate and the angle of attack. In the MPC response, these two are seen to increase initially; whereas the opposite is observed in the LQR control.

This difference is attributed to the fact that MPC considers the future evolution of the dynamics to determine the control law. Thus, MPC bears in mind that the final altitude is 10 metres below the initial altitude, and takes advantage of this extra potential energy to convert it to kinetic energy, which will provide the required acceleration to recover the Δu of -2 m/s. Furthermore, the initial pitch angle is negative, indicating that the aircraft has an initial tendency to loose altitude. As a consequence, the command of MPC to the elevons is to allow the dynamic stability of the phugoid mode (Subsection 2.4.1) to return the aircraft to equilibrium, while ensuring that the overshoot is minimized. In fact, the only difference in behaviour at the initial instants with respect to the time response of the phugoid mode in the absence of controls, Figure 4.1, is the behaviour of the angle of attack, which in the end allows for the non-oscillatory response to equilibrium in the presence of controls.

Bibliography

[1] "Plan Estratégico para el Desarrollo del Sector Civil de los Drones en España 2018-2021," 2018. Ministerio de Fomento, Gobierno de España.

[2] AESA, "Registro de Comunicaciones Previas de Operadores de Aeronaves RPA's," April 23 2018. Ministerio de Fomento, Gobierno de España.

[3] Real Decreto 1036/2017, de 15 de diciembre, por el que se regula la utilizacin civil de las aeronaves pilotadas por control remoto., "Boletín Oficial del Estado, Núm. 316, de 29 de diciembre de 2017, pp 129609 a 129641."

[4] "European Drones Outlook Study. Unlocking the value for Europe," November 2016. SESAR.

[5] O. and W. Wright, "Flying machine," May 22 1906. US Patent 821,393.

[6] B. Etkin and L. D. Reid, *Dynamics of Flight: Stability and Control*. John Wiley & Sons, 1996.

[7] L. Wang, *Model Predictive Control Design and Implementation Using Matlab*. Springer-Verlag, 2009.

[8] E. F. Camacho and C. Bordons, *Model Predictive Control*. Sprringer-Verlag, 2007.